Reconstructing the Tropical Thermocline from Oxygen-Isotopes in Planktonic and Benthic Foraminifera

K. Q. Lakhani[1], J. Lynch-Stieglitz[1], and B. Findley[1]

[1]Georgia Institute of Technology.

Corresponding author: Karim Lakhani (klakhani7@gatech.edu)

Key Points:

- We show a novel method for reconstructing the upper water column using oxygen isotope measurements on multiple species of foraminifera
- This method can be used to quantitatively reconstruct spatial and temporal changes in thermocline depth
- If a simple differencing method is preferred, thermocline depth can be most accurately reconstructed using subsurface species only

In press *Paleoceanography and Paleoclimatology*

Submitted: October 20, 2023

Accepted: April 24, 2024

Abstract

Reconstructing the spatial patterns in thermocline depth is critical for understanding ocean-atmosphere interactions. Previous foraminiferal proxies of thermocline depth focus on gradients between planktonic foraminifera living in the surface and subsurface ocean. However, both thermocline depth changes and stratification changes will impact this measure. In this study, we outline a method for reconstructing the tropical upper ocean vertical water column profile, enabling the separate assessment of thermocline depth and stratification changes. This method uses oxygen isotope data from surface and sub-surface calcifying planktonic foraminifera (*Globigerinoides ruber albus*, *Globorotalia tumida*, *Neogloboquadrina dutertrei*, and *Pulleniatina obliquiloculata*) as well as data from benthic foraminifera from a core site below the thermocline. Using newly generated and compiled oxygen isotope data from Holocene-aged marine sediments, we construct vertical profiles at 20 core sites in the Tropical Pacific Ocean. Quantitative estimates of thermocline depth along with error ranges from Monte Carlo simulations are extracted from the reconstructed profiles. There is a strong correlation between reconstructed Holocene and climatological thermocline depth, but the East-West contrast in the depth of the thermocline is underestimated by 30%. Incorporating benthic information in thermocline estimates results in a dramatic improvement in the reconstruction of spatial gradients in thermocline depth compared to a simpler proxy, the difference in oxygen isotope ratio between a deeper calcifying planktonic species and the surface species, *G. ruber*.

Plain Language Summary

The thermocline is a layer of the ocean where temperature changes rapidly, and the depth of this layer is related to many climatic phenomena. Understanding where and when this layer was deeper and shallower in the past is important to our overall understanding of the climate system. We outline a novel method to reconstruct the thermocline with microscopic shells collected from the sea floor. Our method can reconstruct the changes we see across the Pacific today and also recreate the changes found between the last ice age and today.

1 Introduction

The thermocline is a climatologically important feature of the coupled ocean-atmospheric system, especially in the tropical Pacific. The thermocline is generally shallow in the Eastern Tropical Pacific and generally deep in the Western Tropical Pacific. The Walker Circulation and the El-Nino Southern Oscillation (ENSO) are intimately linked to changes in this East-West thermocline feature (Andreasen & Ravelo, 1997; DiNezio et al., 2011; Vecchi et al., 2006). Model simulations of past climate do not robustly recreate these phenomena, and thus accurate paleoreconstructions of the thermocline are needed to constrain model simulations (DiNezio et al., 2011; Liu et al., 2020; Tian & Jiang, 2020).

Planktonic foraminifera are a commonly used archive to investigate past ocean changes as their calcitic shells can be preserved for millions of years, and the geochemical signals in their shells are directly influenced by overlying ocean properties. Some planktonic foraminifera

calcify in the surface mixed layer (and thus can be used to reconstruct surface conditions) while others calcify deeper in the water column (Fairbanks et al., 1980, 1982). Many thermocline reconstructions are based on the calculation of differences in $\delta^{18}O$ of calcite ($\delta^{18}O_c$) between surface and sub-surface calcifying species (e.g. Cannariato & Ravelo, 1997; Ford et al., 2018; Ford et al., 2012; Ravelo & Andreasen, 1999; Spero et al., 2003). The basis for these techniques is that $\delta^{18}O_c$ predominantly reflects temperature, and that when the thermocline is shallow the difference in $\delta^{18}O_c$ for the surface and deeper dwelling species will be greater. Similar approaches use Mg/Ca based temperature reconstructions in deep and shallow dwelling planktonic species (e.g., Ford et al., 2015; Hollstein et al., 2020; Hollstein et al., 2018). Qualitative reconstructions of thermocline depth based on this concept have been key to establishing the timing of the onset of the modern East-West tilt associated with a strong Walker circulation over time scales of several million years (Wara et al., 2005), and have been used to detect thermocline changes associated with the Last Glacial Maximum (Ford et al., 2018; Leech et al., 2013; Loubere, 2001; Patrick & Thunell, 1997).

However, the difference in $\delta^{18}O_c$ between surface and subsurface species can vary independently of thermocline depth. Changes in surface water properties alone, with no change below the mixed layer can influence the surface-subsurface difference. This can be seen in regions with large spatial gradients in vertical stratification of the water column that are driven by freshwater input at the surface. In these regions, the temperature and $\delta^{18}O_c$ differences between surface and subsurface species can reflect those changes in stratification as opposed to changes in the depth of the thermocline. For example, in the Eastern Tropical Pacific, the thermocline depth is similar north and south of the equator. However, surface waters north of the equator are warm and fresh, whereas to the south they are cold and salty. Driven by the surface water properties, there is a large difference in the surface to subsurface $\delta^{18}O$ gradient across the front separating these two regimes, despite the similar thermocline depth (Rincón-Martínez et al., 2011). While lines of evidence can be used to assume one component is small relative to the other, this evidence must be local, making cross-basin comparisons and interpretation tricky (Cannariato & Ravelo, 1997; Ford et al., 2015).

Here, we propose a multi-species regression approach to reconstructing the water column $\delta^{18}O$ profile between 0 m and 600 m, incorporating $\delta^{18}O_c$ data from planktonic and benthic foraminifera that have calcified at different depths in the water column. Because we reconstruct the vertical profile of the water column, we are able to separately assess changes in surface water properties (stratification) and thermocline depth changes. These profiles are in $\delta^{18}O$ space, but because the dominant control on the vertical profile of $\delta^{18}O$ in the tropics is temperature, this method can be used to reconstruct quantitatively the depth of the thermocline along with an error range. We examine how the thermocline depth reconstructed using the regression method from Holocene aged sediments in the Tropical Pacific matches the climatological thermocline depth, and explore how the method can be used to reconstruct differences in thermocline depth over time. Finally, we test the traditional differencing methods

using our data set, and propose a new differencing method using only subsurface species which improves the correlation to thermocline depth.

2 Materials and Methods

2.1 Foraminiferal Oxygen Isotope Data

For this work, we require oxygen isotope data from four sub-surface species of foraminifera: *Globigerinoides ruber albus* (henceforth *G. ruber*), *Globorotalia tumida*, *Neogloboquadrina dutertrei*, and *Pulleniatina obliquiloculata*. Our previously compiled core top and Holocene aged planktonic foraminifera data set from the global tropics (Lakhani et al., 2022) had six Tropical Pacific sites for which Holocene dated (0-6ka) data exist for all four species (Ford et al., 2018; Hollstein et al., 2017) (Table 1). We supplement this data with newly generated oxygen isotope data for subsurface-dwelling species for 14 additional Late Holocene and Mid Holocene dated cores in the Tropical Pacific, for which data on some of the species already had been generated (Koutavas & Lynch-Stieglitz, 2003; Leech et al., 2013; Lynch-Stieglitz et al., 2015; Monteagudo et al., 2021).

The age models for these 14 additional cores were updated using existing radiocarbon data, INTCAL20 and PaleoDataView to ensure that the core depths were accurately dated (Langner & Mulitza, 2019; Reimer et al., 2020). The reservoir age was determined from simulations done in (Butzin et al., 2017). If the grid point did not have a reservoir age, the nearest grid cells were checked for a reservoir age, with increasing distance to the core location. Linear interpolation and extrapolation were used to estimate ages for core depths between those with measured radiocarbon dates. The radiocarbon data used for the age models is in Table S1. $\delta^{18}O_c$ measurements were conducted on a Thermo MAT253 Stable Isotope Mass Spectrometer coupled to a Kiel IV Carbonate Device at Georgia Tech. *G. tumida* was picked from the 425-500 µm size fraction and measured in groups of 1-2 shells. *N. dutertrei* was picked from the 355-425 µm size fraction and measured in groups of 2-5 shells. *P. obliquiloculata* was picked from the 355-425 µm size fraction and measured in groups of 2-7 shells. $\delta^{18}O_c$ measurements were converted to PDB using an in-house standard and NBS-19. The $\delta^{18}O$ of NBS-18 was also monitored. Reproducibility of the in-house standard was 0.059‰ for $\delta^{18}O$ and 0.020‰ for $\delta^{13}C$ (1 sigma). The data for individual measurements is in Table S2, and the Holocene average $\delta^{18}O_c$ are shown in Table 1 and Figure 1a-d, along with the previously published data. The averages for each species at each core site (Table 1, Figure 1a-d) include data points dated to 0-6 ka for both new and previously published analyses. The total number of analyses contributing to each data point are reported in Table S3. We choose not to add any species-specific offsets to the planktonic foraminifera data, consistent with Lakhani et al. (2022), since we will be using apparent calcification depths from that study.

We also use $\delta^{18}O_c$ from benthic foraminifera at a single core site, KNR195-5 GGC43 (Bova et al., 2015, 1.25°S, 89.68° W, 617m) to constrain the bottom of the regressions for this region. The data was generated on *Uvigerina peregrina*, which has a species-specific offset of

0.47‰ from the (Kim & O'Neil, 1997) paleotemperature equation (Marchitto et al., 2014). The average $\delta^{18}O_c$ for this species between 0-6ka is 2.22‰. After adjusting for this offset, $\delta^{18}O_c$ is 1.75‰, very close to the expected value from climatology of 1.63‰ calculated using the climatological temperature (Locarnini et al., 2013) and $\delta^{18}O_{sw}$ (LeGrande & Schmidt, 2006) and the paleotemperature equation from Kim and O'Neil (1977) at the core site.

2.2 Regression-based Water Column Profile Reconstruction

To create a profile from the individual data, we first define a functional form of the predicted $\delta^{18}O_c$ vertical profile. Qualitatively, in the open ocean, there is a surface mixed layer where $\delta^{18}O$ (and other oceanographic variables such as temperature and density) change very slowly with depth, followed by a sharp change in $\delta^{18}O$ indicating the thermocline/pycnocline, below which oceanographic variables change much more slowly. To model this quantitatively, we define a mixed layer that extends to some depth MLD where $\delta^{18}O_c(z)$ is held constant, followed by an exponential curve that rapidly increases in $\delta^{18}O_c$ with depth before approaching an asymptotic deep ocean $\delta^{18}O_c$ value of β_3 (Equation 1).

$$\delta^{18}O_c(z) = \begin{cases} C_1 & z \le MLD \\ (-1) * \beta_1^{(-1)*(z+\beta_2)} + \beta_3 & z \ge MLD \end{cases} \qquad (Eq.\,1)$$

Figure S1 shows how the reconstructed profile is impacted by each parameter. For each core site, the best fit parameters for the model are determined using the $\delta^{18}O_c$ data from the planktonic foraminifera for that site paired with the average Apparent Calcification Depth (ACD) for that species from Lakhani et al. (2022) and the $\delta^{18}O_c$ from benthic foraminifera from a core in the Eastern Tropical Pacific at 617 m water depth. Over the Tropical Pacific (20°S-20°N, 140°E-80°W), below 600m, there is little variance in predicted $\delta^{18}O_c$ over the basin. Thus, for core locations with a water depth of more than 600m, we can use the benthic foraminifera $\delta^{18}O_c$ from any core in this domain. Through much of this domain, the error in using benthic $\delta^{18}O_c$ from a different site as compared to the true value at a site is less than 0.2‰, and for the core sites considered here is always less than 0.1‰ (Figure 1e).

C_1 is assigned the value of the $\delta^{18}O_c$ of the surface-dwelling species *G. ruber. G. ruber* has an ACD of 17 m and has been used to reconstruct surface properties of the ocean (Lakhani et al., 2022). Data from the other three planktonic species and the benthic value are used to estimate the parameters $\beta_1, \beta_2,$ and MLD using a root-mean-squared cost function. With the condition that the regression is continuous at the mixed layer, β_3 is fixed at $\beta_3 = C_1 + \beta_1^{-(MLD+\beta_2)}$. Starting with plausible ranges for these four parameters, every parameter combination is evaluated. The calculated $\delta^{18}O_c(z)$ is compared to the measured $\delta^{18}O_c$ at the average ACD of each species (210 m for *G. tumida*, 114 m for *N. dutertrei* and 94 m for *P. obliquiloculata*), and at the depth of the core (617 m) for the benthic data point. The best fitting parameters minimize the root-mean-squared distance between these four species' $\delta^{18}O_c$ and the predicted $\delta^{18}O_c$ at that species' average ACD. This parameter estimation is done first at a coarse resolution in parameter space

and then at a fine resolution to optimize speed and accuracy. For example, for MLD, if the optimal regression has a MLD of 47 m, the parameter estimation would evaluate possible parameters between 20 and 140 m every 15 m, identify that the best choice is between 35 and 50 m, and then at a finer resolution, evaluate parameters between 35 and 50 m. The code for this model is uploaded on Github.

To handle the uncertainty in planktonic foraminiferal ACD, we sample from the distribution of ACD for each species in (Lakhani et al., 2022). The model is fit to these realized ACD values many times in a Monte-Carlo style to produce a cloud of realizations. The resulting cloud gives a lower-bound on the uncertainty in the regression, as there are other sources of uncertainty not incorporated in these simulations.

For validation of this model, at each core site we calculate the vertical profile of predicted foraminiferal $\delta^{18}O_c$ using the World Ocean Atlas 2013 mean annual temperature climatology (Locarnini et al., 2013), the $\delta^{18}O_{seawater}$ climatology from (LeGrande & Schmidt, 2006), and the linear paleotemperature equation from (Kim & O'Neil, 1997; Lynch-Stieglitz et al., 1999). While there may well be species specific disequilibrium effects, they are poorly known for subsurface species (Lakhani et al., 2022 and references therein). Assuming that all tropical planktonic species follow the equation based on Kim & O'Neil (1997) leads to a calculation of reasonable ACD (Lakhani et al., 2022), and we follow that approach here for consistency as we use the ACD from that study in the regression analysis.

3 Results and Discussion

This work uses data from 20 core locations; 6 locations are in the Eastern Tropical Pacific, 5 locations are in the Central Tropical Pacific, and 9 locations are in the Western Tropical Pacific. This allows us to evaluate how well our model reconstructs the predicted $\delta^{18}O_c$ profile across a wide range of oceanographic conditions. The core locations and $\delta^{18}O_c$ data for this analysis are shown in Table 1. The $\delta^{18}O_c$ is plotted spatially in Figure 1a-d.

3.1 Water Column Profile Reconstructions

Representative profiles generated from the foraminiferal data are shown in Figure 2, and profiles for all sites are shown in Figures S2-S5. There is broad agreement between the planktonic foraminiferal data and the modeled profile in all cases, with the individual Monte Carlo runs of the model surrounding the profile generated from the average species-specific ACD's. This means that the form of the regression is flexible enough to model the data from the different regions, and the large-scale differences between the Eastern and Western Tropical Pacific seen today (Figure 2). However, the observed climatological profile does not completely fall within the Monte Carlo cloud of the regression produced by the method. The limitations of the assumed exponential form preclude the possibility of capturing the more complex structure in the Eastern Tropical Pacific and the water column above the thermocline in the Central and Western Tropical Pacific.

The inclusion of benthic $\delta^{18}O_c$ data is critical to the success of the method (Figure 2 and Figure S2-S5). Benthic foraminifera live at a known depth and have smaller $\delta^{18}O_c$ variance than planktonic foraminifera due to living in the deep ocean, where temperature is less variable. This allows the regression to be anchored by a datapoint that is known to higher accuracy than any of the subsurface planktonic species. This is particularly important for exponential functions that have an asymptote; a change in the deepest datapoint has a direct impact on the $\delta^{18}O_c$ of the asymptote and thus the shape of the upper part of the regression. Including accurate benthic data makes the regression much more accurate overall, both below the depth of *G. tumida*, the deepest living planktonic species, and above this depth.

3.2 Limitations of Profile Reconstructions

While this method seems promising, there are limitations in its use for estimating vertical water column profiles during the past. Firstly, this method is inherently limited by the accuracy at which we know the calcification depths of the foraminifera. Reducing the error in the ACD of these species reduces the Monte Carlo error around the mean regression, which affects the magnitude of thermocline change that can be estimated from this method. If the thermocline change is subtle between two time periods, the signal would be too small relative to the noise from the uncertainty in depth habitat, resulting in a conclusion of no significant change between the time periods. We have also previously demonstrated that for some subsurface species, the ACD can depend on thermocline depth. We can see this in our data in Figure 1, where the foraminiferal $\delta^{18}O_c$ values for *N. dutertrei* and *P. obliquiloculata* are lower than the values at the ACD (warmer values) in the east, and higher (colder values) in the west. This method does not incorporate this dependence, using the full modern range of ACD across the global tropics when calculating the Monte Carlo clouds.

This method also uses a simple form of the upper ocean that is not always a good estimate for the real profile. The simple form is required to limit the number of free parameters given the small amount of data available to constrain the regression. In regions where this is not a good approximation of reality, the model would systematically differ from reality. For example, there are systematic differences between the regression and the profiles calculated using climatological temperature and $\delta^{18}O_{sw}$ in cores from the Eastern Tropical Pacific below 200 m due to the simplicity of the functional form. While the model broadly matches the profiles calculated from climatological values despite this, this method cannot necessarily be applied wholesale to a different region. Depending on the interplay between subsurface water masses affecting a local profile, this method would not be suitable for reconstructing the water column profile. Along with this, if the typical vertical structure in the water column $\delta^{18}O_c$ in a region is significantly different in the past, this method would need to be modified to match those conditions.

We also note that the method, as applied, results in a vertical profile of $\delta^{18}O_c$, which reflects both $\delta^{18}O_{sw}$ and temperature. Depending upon the application, the desired reconstruction

might be a vertical profile of temperature; In that case, paleo-temperature proxies such as Mg/Ca on foraminifera could be used in a similar manner. However, in other applications, a vertical profile of density might be most relevant, in which case the $\delta^{18}O_c$ profile might be more useful since both temperature and salinity (correlated with $\delta^{18}O_{sw}$) influence density (Lynch-Stieglitz et al., 1999).

3.3 Thermocline Depth from Profile Reconstructions

We compare estimates of the thermocline depth derived from the model to the climatological thermocline depth. We use the depth of the 20°C isotherm, an often used proxy for the thermocline depth, as it is the depth that corresponds to strongest temperature gradients in today's tropical ocean. We derive an equivalent measure to the 20°C isotherm that can be used for our reconstructed $\delta^{18}O_c$ profiles. We calculate the $\delta^{18}O_c$ that corresponds to the 20°C isotherm in today's ocean to be the depth where $\delta^{18}O_c(z) = \delta^{18}O_c(T = 20℃, \delta^{18}O_{sw} = 0.36‰) = -0.66‰$, with 0.36‰ being the average $\delta^{18}O_{sw}$ in the tropical Pacific at 150 m. The depth of this $\delta^{18}O_c$ value calculated from climatological $\delta^{18}O_{sw}$ and T is at all locations very close in depth to the 20°C isotherm (Figure S6). We then can compare the depth in the regression at which $\delta^{18}O_c = -0.66‰$ directly to the 20°C isotherm (Table 2, Figure 3, Figure 4). The thermocline estimates using this metric derived from the regression model are well correlated with the depth of the climatological 20°C isotherm, but with a slope less than one (0.7), indicating a systematic overestimation of thermocline depth in locations where the thermocline is shallow and underestimation where it is deep . The thermocline depth reconstructed in the Western Tropical Pacific is systematically too shallow by 26 m (Figure 3), but agrees with the climatological value, within the error envelope from the Monte Carlo simulations. The reconstructed thermocline depth is on average 35 m deeper than observed in the Eastern Tropical Pacific (Figure 3, Figure 4, Table 2). The disagreement in the Eastern Tropical Pacific stems, at least in part, to the fact that the actual vertical profile has a more complicated shape than our regression model. Forcing the data to the exponential shape results in these slightly too deep thermocline depth estimates. Another factor leading to the reduced east-west contrast in thermocline depth is that there is systemic spatial variation in the ACD, with both *N. dutertrei* and *P. obliquiloculata* calcifying at more shallow depths where the thermocline is shallow. In this study, we sampled the entire ACD distribution from today's tropical ocean, including Pacific, Atlantic and Indian Oceans at all core locations. While we could have improved the agreement with climatology if we used regional ACD, for paleoclimate applications we would not know *a priori* which regional distribution would be most appropriate at each location. Further refinements of the method which account for the correlation of ACD thermocline depth may be possible. But, overall, the method is doing a good qualitative job reconstructing the thermocline depth of the 20°C isotherm over the entire region, as evidenced by the strong correlation shown in Figure 4. The method also provides a quantitative estimate of thermocline depth consistent with observed values, albeit with a large error range as well as systematic errors related to thermocline depth.

3.4 Application to the Last Glacial Maximum

We apply our method using previously published data for the Last Glacial Maximum in the Eastern Pacific. Ford et al. (2018) have reported data at core ODP 849 (0.183°N, 110.519°W, 3,839 m water depth) for the species used in our analysis for the Holocene and the LGM. The benthic record from (Bova et al., 2015) extends through the LGM, and so we use the average $\delta^{18}O_c$ for *U. peregrina* between 19 ka and 23 ka adjusted for its species-specific offset for the benthic data point (2.79‰). Taking into account the sea level difference between the LGM and modern, we shift the benthic depth 121 m shallower in the water column to 496 m (Fairbanks, 1989). While this is shallower than the benthic data we use for the Holocene, because both cores are in the Eastern Pacific, we assume that benthic data from core KNR195-5 GGC43 is representative of conditions at the same water depth at the location of ODP849. No adjustment in the planktonic species ACD is needed as these species freely float in the upper ocean.

Once the overall increase in $\delta^{18}O_c$ due to ice volume change and cooling is accounted for, the regression method suggests a deepening of the thermocline (Figure 5). The average profile for the LGM is deeper than the average profile for the Holocene, with much of the Monte Carlo cloud being deeper as well. While there is a systematic deepening caused by the *G. ruber* data for the LGM having a lower $\delta^{18}O_c$ after the ice volume and SST adjustment, even when aligned, the average LGM profile has a deeper thermocline than the average Holocene profile. Another difference between the two profiles is the difference in the depth of the benthic data. However, the use of shallower benthic data to constrain the profile would lead to a shoaling of the profile, all else being equal, making any signal of a deeper thermocline an underestimate. Despite differences in applying this method to the LGM that could skew comparisons, we find a deeper thermocline at this core location during the LGM, in line with previous interpretations of this data.

Using our thermocline metric of $\delta^{18}O_c$ = -0.66 we assess the Holocene depth of the thermocline to be 57 m (48-96 m 95% confidence interval from Monte Carlo simulations). For the Holocene, we chose this thermocline metric because it best approximates the depth of the 20°C isotherm which, in turn, is co-located with the highest vertical temperature gradient in the modern ocean. Our regression method, which assumes an exponential form, cannot tell us which isotherm (or level of constant $\delta^{18}O_c$) is collocated with the highest vertical temperature gradient in the glacial ocean. So, in the absence of an alternative, we assume a similar overall vertical water column structure, once the overall cooling (2.5°C*0.21=0.525‰) (Monteagudo et al., 2021) and higher $\delta^{18}O$ (1.0‰)(Schrag et al., 2002) is accounted for. Under this assumption our glacial thermocline metric becomes 0.87‰. Using this metric, we calculate a thermocline depth of 89 m (57-121 m 95% confidence interval from Monte Carlo simulations). We now have a quantitative estimate 30 meter lowering with quantified (and large) uncertainty ranges. We can use these ranges to estimate a 93% likelihood that the thermocline was deeper during the LGM.

Our finding that the thermocline was likely deeper is consistent with the interpretation in the original paper where the data was published. Ford et al. (2018) found that the vertical

gradient between the surface species and the subsurface species decreased during the LGM, which they interpret as consistent with a deepening of the thermocline. While changes in upper ocean stratification could result in a similar signal in difference in the $\delta^{18}O_c$ of these species, the authors cite evidence that this was not an important factor at this site (Cannariato & Ravelo, 1997; Ford et al., 2012). However, in our approach we incorporate the information that the $\delta^{18}O_c$ gradient between the subsurface planktonic foraminifera and the benthic foraminifera decreased at the same time as the surface-subsurface gradient increased. This enhances confidence in the interpretation that the thermocline was deeper, and that changes in surface stratification were not driving the changed surface-subsurface gradient.

3.5 Species difference-based thermocline depth proxies

With this dataset, we can investigate the effectiveness of the difference between *G. ruber* and *G. tumida* $\delta^{18}O_c$ as a proxy for thermocline depth. The difference between $\delta^{18}O_c$ of *G. ruber* and *G. tumida* is a commonly used metric for understanding upper ocean changes (Cannariato & Ravelo 1997, Rincon-Martinez et al. 2011, Ford et al. 2018). The differencing removes mean ocean differences over the domain of interest. For example, if the whole ocean warms or freshens uniformly, all else being equal, this difference between the data from surface and subsurface species remains constant. Any additional changes can be influenced by changes in the water column profile. However, a change in the surface processes setting *G. ruber* $\delta^{18}O_c$ and surface to subsurface stratification is indistinguishable in its influence on the proxy from a change in the thermocline depth. The Holocene *G. ruber* - *G. tumida* $\delta^{18}O_c$ is not well correlated to modern thermocline depth at the sites in our study (Figure 6a), suggesting a large role for stratification changes. Using the other subsurface species instead of, or in addition to, *G. tumida* only improves the correlation slightly (Figure 6b-d).

The much stronger correlation of reconstructed thermocline depth using our regression method (Figure 2) is likely driven by the inclusion of the $\delta^{18}O_c$ data from benthic foraminifera. We therefore propose comparing *G. tumida* (or other subsurface dwelling species) $\delta^{18}O_c$ to a benthic species $\delta^{18}O_c$ as an alternative to the *G. ruber*-*G. tumida* $\delta^{18}O_c$ difference. When differenced from the benthic instead of *G. ruber* $\delta^{18}O_c$ data, the relationship to thermocline depth is much stronger and consistent across the species (Figure 7). Despite each species calcifying at a different ACD and the significant variance within each species, the relationship between these difference measures and the thermocline depth is strong. In addition to this, the difference using the average of all three species is even more highly correlated to thermocline depth than any single species, with the same R value as the correlation using the full profile (Figure 2).

The same benthic data is used for all sites, meaning that *G. tumida, N. dutertrei,* and *P. obliquiloculata* $\delta^{18}O_c$ and their mean $\delta^{18}O_c$ are correlated with thermocline depth, even if they are not differenced to the benthic data. So what is gained by using the data from the benthic foraminifera? If we would like to apply these relationships as a proxy for thermocline depth

back in time, rather than just in space as we do here, we need to incorporate the information provided by the benthic foraminifera. By differencing the data from the subsurface planktonic foraminifer from the benthic data at 600 m, we eliminate from consideration changes over time in temperature and $\delta^{18}O_{sw}$ which impact both the subsurface planktonic and the benthic data. This will ensure that the proxy is measuring only the vertical difference in $\delta^{18}O_c$ between the depths at which the foraminifera calcified. Cannariato & Ravelo (1997) used a similar approach, comparing the difference in *G. tumida* and the mixed layer species *T. sacculifer* $\delta^{18}O_c$ to the difference in these species $\delta^{18}O_c$ with benthic data from a nearby core in order to isolate surface influences on the *G. tumida-T. saccculifer* difference over the past 5 Ma.

4 Conclusions

We present a novel regression method that incorporates the $\delta^{18}O_c$ of multiple species of planktonic foraminifera and benthic foraminifera to quantitatively reconstruct the vertical water column profile. New $\delta^{18}O_c$ measurements for *G. tumida, N. dutertrei,* and *P. obliquiloculata* allow us to apply this method to the Tropical Pacific, and demonstrate that the first order differences in the vertical water column profile between the regions is captured by the method. We use the information from the profiles to infer thermocline depth. While the reconstructed thermocline depth is highly correlated to the actual thermocline depth, there are systematic differences with an overestimation of thermocline depth where the thermocline is shallow and underestimation of the thermocline depth where the thermocline is deep. This method provides a quantitative estimate of thermocline depth, with an error envelope provided by the Monte Carlo simulation. Such error estimates can be useful when incorporating paleoclimate data into data assimilation or inverse modelling reconstructions of past climate states.

By including data from both surface and subsurface planktonic foraminifera, as well as benthic foraminifera at a site below the thermocline, this method can capture both changes in stratification (through the difference between surface water and subthermocline properties) and thermocline depth (through the relationship between the properties captured by the sub-surface planktonic foraminifera). The ability of the regression method to provide information on both changes in stratification and thermocline depth provides an improvement on the commonly-used approach of differencing the $\delta^{18}O_c$ of *G. ruber* and *G. tumida* (or other subsurface calcifying foraminifera) which could reflect either changes in stratification or thermocline depth. If a simple differencing method for reconstructing thermocline depth is desired, differencing the $\delta^{18}O_c$ from subsurface species from benthic foraminifera $\delta^{18}O_c$ instead of *G. ruber* provides a more robust proxy.

While the regression method represents a positive step towards quantitative estimates of thermocline depth and other aspects of the upper ocean water column, the large Monte Carlo error estimates provide a reminder that quantitative does not necessarily mean precise. It is our hope that improved understanding of planktonic foraminifera calcification depth, the use of

multiple proxies, information from individual foraminifera, and method improvements will lead to more precise reconstructions in the future. However, even with the current state of knowledge, our regression method might prove useful for studies where there is interest in both surface stratification and thermocline depth.

Acknowledgments

This work was supported by the National Science Foundation (OCE-1502927, OCE-2002297). We thank the reviewers for their helpful comments which have greatly improved the manuscript.

Open Research

The data used in the study are available at in Tables 1 and S2. The code for generating the figures is available through Zenodo and Github (Lakhani, 2024). The preserved release is located here: https://github.com/lakhani1118/Thermocline_Reconstruction/releases/tag/tag1.

5 Figures and Tables

Table 1: Core Locations and Holocene Average $\delta^{18}O_c$

Core name	Latitude (°N)	Longitude (°E)	Depth (m)	G. ruber $\delta^{18}O_c$ (‰)	G. tumida $\delta^{18}O_c$ (‰)	N. dutertrei $\delta^{18}O_c$ (‰)	P. obliq $\delta^{18}O_c$ (‰)
GeoB17421-2	-3.55	144.20	588	-3.45	-0.31	-1.39	-2.20
GeoB17419-2	-2.81	144.50	1887	-3.09	-0.50	-1.64	-1.76
GeoB17430-2	-4.22	145.03	1160	-3.09	-0.01	-1.75	-2.15
GeoB17429-1	-4.10	145.20	1604	-3.02	-0.07	-2.01	-2.00
GeoB17435-2	-7.27	147.34	1001	-3.29	-0.15	-2.09	-2.23
VM24-150	-2.20	155.70	1849	-2.48	-0.99	-0.97	-1.37
VM28-234	-7.13	158.97	2719	-2.60	-1.10	-1.73	-1.40
VM28-235	-5.45	160.48	1746	-2.42	-1.27	-0.89	-1.46
VM28-233	-6.32	161.38	2334	-2.41	-0.98	-1.15	-1.26
ML1208-28BB	2.97	-159.20	3153	-1.74	-0.58	-0.82	-1.39
ML1208-20BB	1.27	-157.26	2850	-2.10	-0.82	-0.94	-1.28
ML1208-19GC	0.83	-156.87	2956	-2.04	-0.51	-0.50	-1.07
ML1208-18GC	0.59	-156.66	3362	-2.10	-0.41	-0.47	-1.05
ML1208-13BB	-0.22	-155.96	3050	-1.91	-0.52	-0.66	-1.08
ODP 849	0.18	-110.52	3839	-1.51	0.60	0.56	-0.33
V21-40	-5.52	-106.77	3182	-1.53	0.63	-0.06	-0.48
RC13-140	2.87	-87.75	2246	-2.60	0.59	0.21	-0.94
RC8-102	-1.42	-86.85	2180	-1.78	0.67	0.56	0.13
RC11-238	-1.52	-85.82	2573	-1.60	0.09	0.48	-0.10
V19-27	-0.47	-82.07	1373	-2.17	0.51	0.66	-0.20

420 Table 2. Reconstructed thermocline depth
421

Corename	Latitude (°N)	Longitude (°E)	Climato-logical Z20 (m)	Calculated Z20 (m)	Standard deviation (m)	2.5 and 97.5 percentile (m)
GeoB17421-2	-3.55	144.20	185	155	27	[109, 208]
GeoB17419-2	-2.81	144.50	186	166	28	[113, 213]
GeoB17430-2	-4.22	145.03	186	152	30	[97, 207]
GeoB17429-1	-4.10	145.20	186	161	29	[105, 214]
GeoB17435-2	-7.27	147.34	186	167	28	[107, 222]
VM24-150	-2.20	155.70	185	163	20	[122, 200]
VM28-234	-7.13	158.97	208	188	23	[140, 238]
VM28-235	-5.45	160.48	205	175	17	[134, 212]
VM28-233	-6.32	161.38	206	164	19	[128, 195]
ML1208-28BB	2.97	-159.20	147	144	21	[108, 197]
ML1208-20BB	1.27	-157.26	140	154	20	[107, 191]
ML1208-19GC	0.83	-156.87	140	131	19	[92, 159]
ML1208-18GC	0.59	-156.66	140	124	21	[85, 165]
ML1208-13BB	-0.22	-155.96	143	132	15	[103, 169]
ODP 849	0.18	-110.52	50	58	12	[47, 94]
V21-40	-5.52	-106.77	79	70	20	[49, 137]
RC13-140	2.87	-87.75	48	87	14	[70, 124]
RC8-102	-1.42	-86.85	29	60	6	[53, 76]
RC11-238	-1.52	-85.82	29	64	9	[52, 87]
V19-27	-0.47	-82.07	33	69	7	[60, 90]
ODP 849 (LGM)	0.18	-110.52	N/A	89	19	[57, 129]

422
423

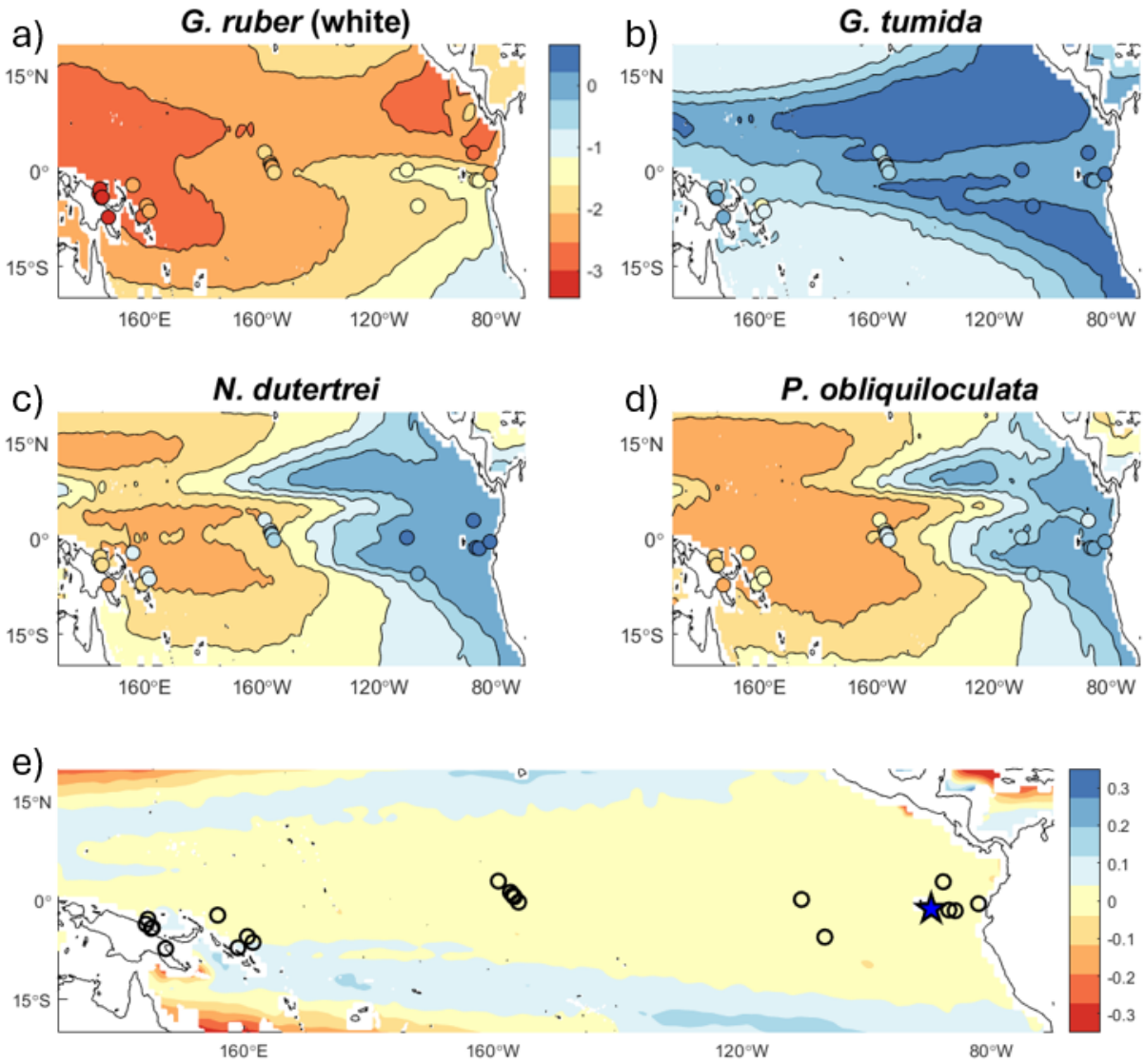

Figure 1: Planktonic foraminifera data and location of benthic core. a) *G. ruber* $\delta^{18}O_c$ for this dataset (filled circles) and climatological $\delta^{18}O_c$ at the *G. ruber* ACD. b) same for *G. tumida* c) same for *N.dutertrei* d) same for *P. obliquiloculata.* e) Location of the core for the 600 m benthic foraminifera (*U. peregrina*) data used for this study (star). Background color is the difference between predicted $\delta^{18}O_c$ at 600 m relative to the core site of the *U. peregrina* data. Core locations for the planktonic foraminifera are shown in the open circles.

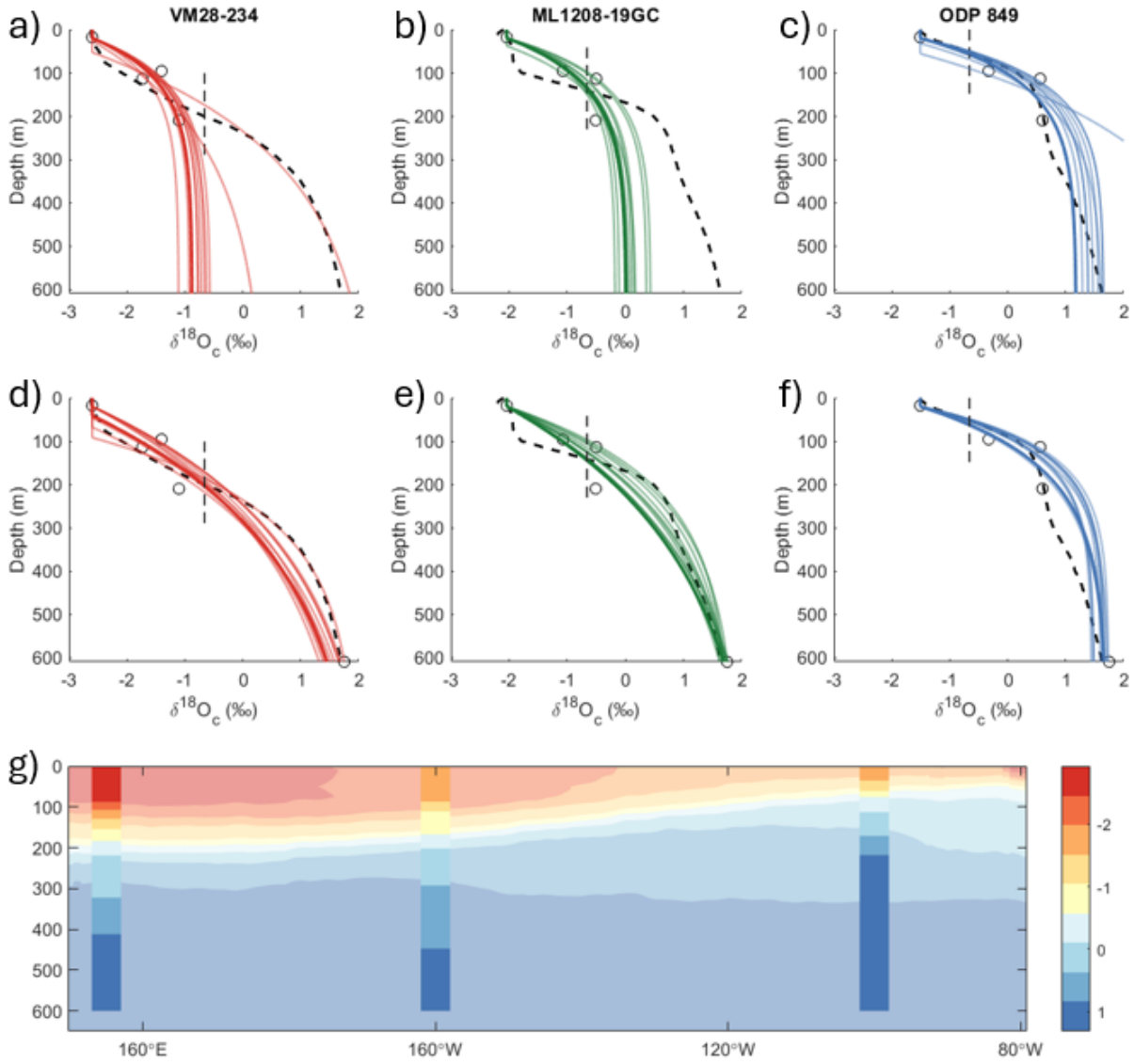

Figure 2: Model results for sample Tropical Pacific cores. a-c) Model results for VM28-234 (Western Tropical Pacific), ML1208-19GC (Central Tropical Pacific), and ODP 849 (Eastern Tropical Pacific) when not including benthic data. Solid line indicates average profile, and lighter lines indicate Monte Carlo error due to ACD variability. d-f) Same as a-c) when benthic data is included. g) Transect plot for Equatoial Pacific. Background is modern climatology-derived $\delta^{18}O$ averaged over 5°S and 5°N. Bars are average of regressionsin each region within this latitude band.

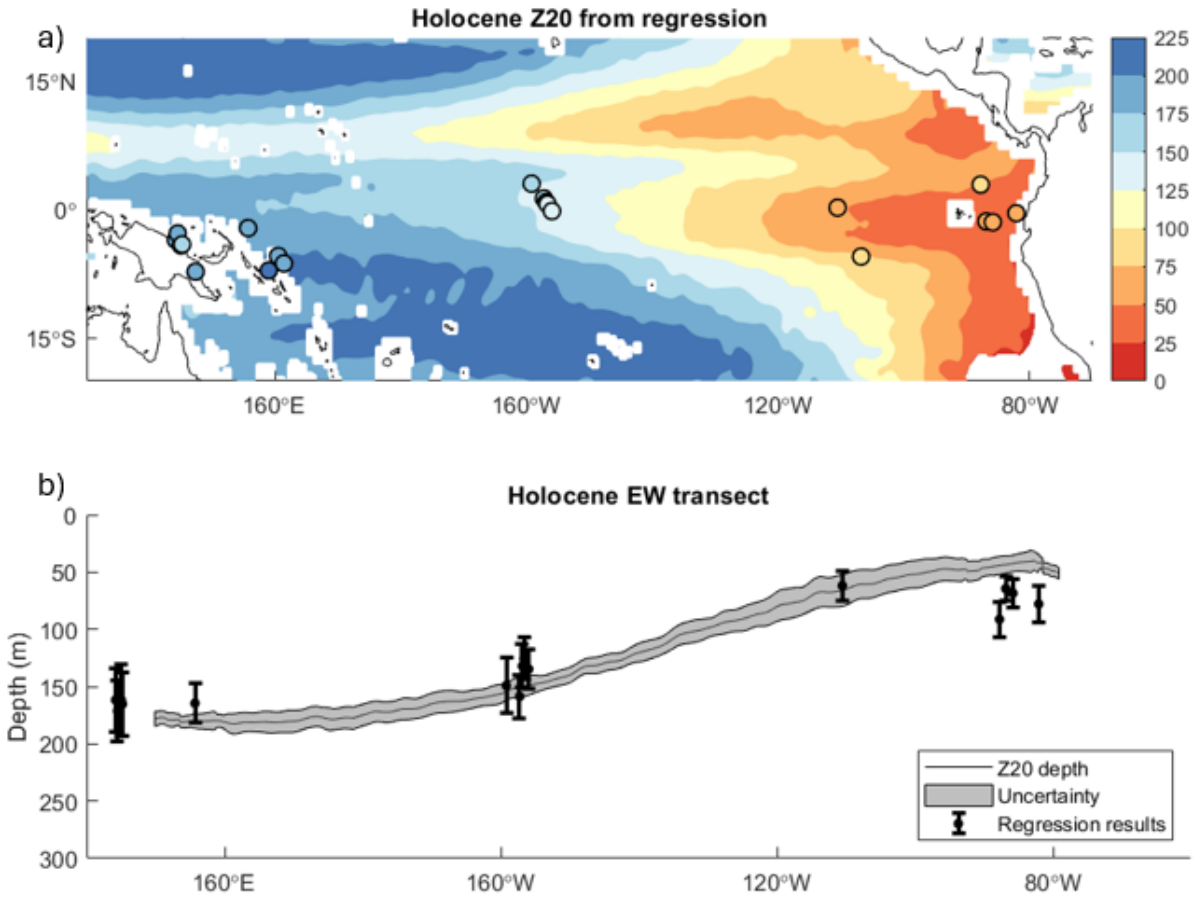

Figure 3: Thermocline depth predicted from $\delta^{18}O_c$ profile. a) depth of Z20 derived from regression for core locations. Contours are Z20 equivalent depth from climatology-based $\delta^{18}O_c$ field. b) average thermocline depth across the equatorial Pacific. Solid line is average Z20 equivalent depth between 5°S and 5°N, and the error envelope represents 1-sigma standard deviation of this depth. Mean regression results are shown as dots, with standard deviation of Z20 equivalent depth as error bars.

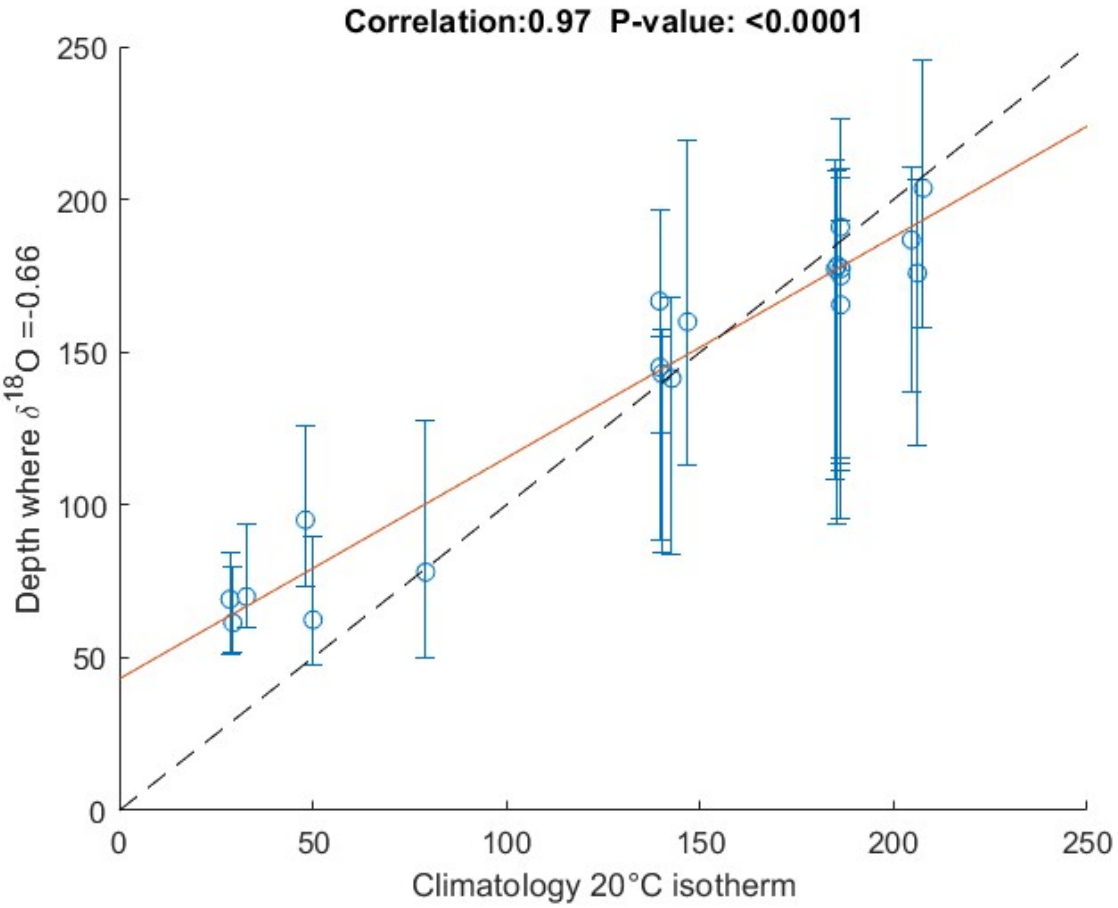

Figure 4: Thermocline depth predicted from $\delta^{18}O_c$ profile. Climatology 20°C isotherm depth (x-axis) compared to the depth where $\delta^{18}O_c = 0.66‰$ as an equivalent measure from the reconstructed $\delta^{18}O_c$ profile (y-axis). Dashed line is the 1:1 line. Error bars are the 95% confidence intervals from the Monte Carlo simulations. While predicted thermocline depth is well correlated with observed depth (R = .97, p<.0001), thermocline depth is overestimated where the thermocline is shallow.

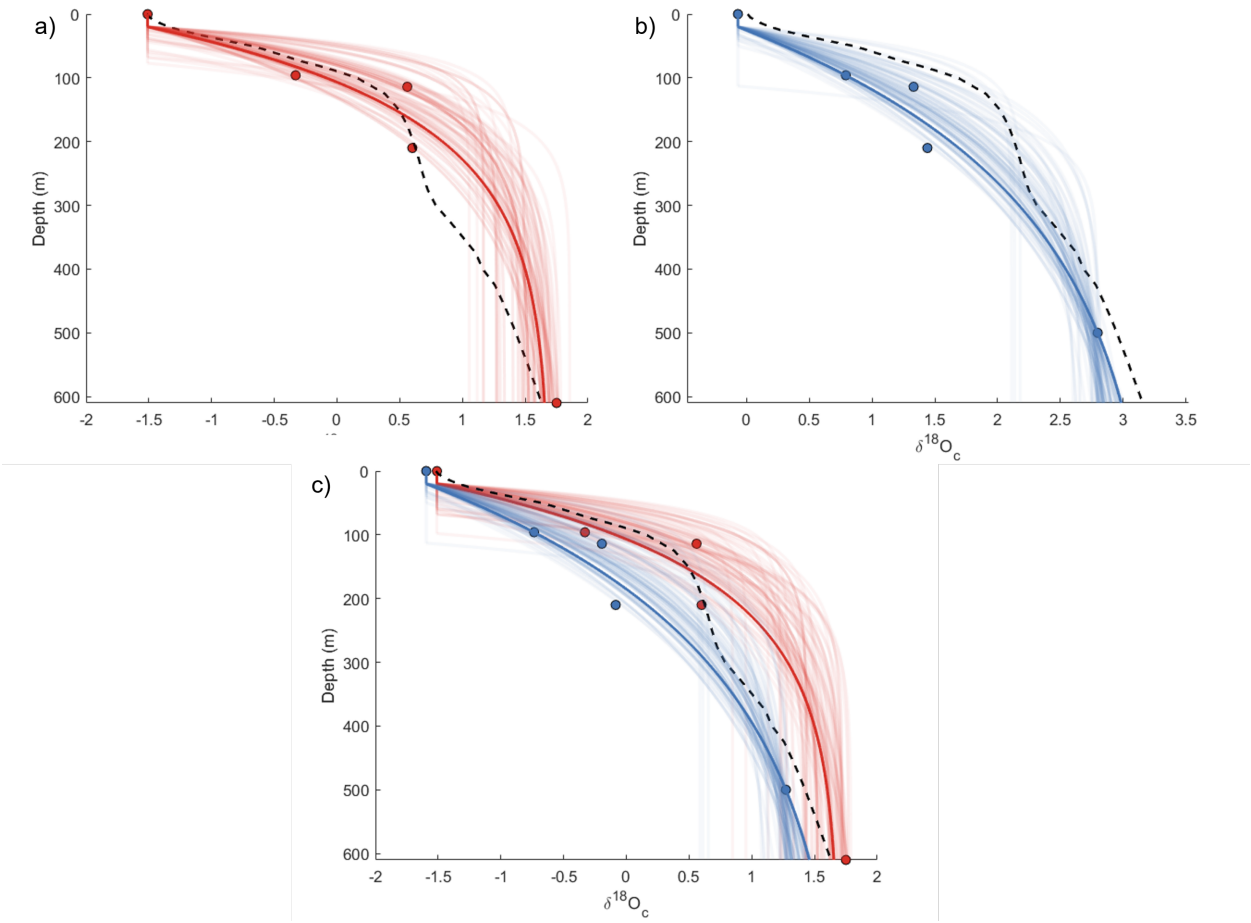

Figure 5: Thermocline model reconstructions for ODP849 for the Holocene and LGM. a) Holocene data from Ford et al. (2018) plotted in circles, with predicted $\delta^{18}O_c$ climatology plotted in black and modeled profile in red. Monte Carlo error due to variability in lighter lines. b) LGM data from Ford et al. (2018) plotted in circles with predicted $\delta^{18}O_c$ climatology plotted in black and modeled profile in blue. Monte Carlo error due to variability is in lighter lines. The climatology profile is shifted by the ice volume change (1.0‰) and SST change applied uniformly (2.5°C*0.21=0.525‰) to align with LGM data and regression (Monteagudo et al., 2021; Schrag et al., 2002). c) LGM and Holocene data and modeled profiles plotted together for comparison. LGM data and regression profile shifted by ice volume change and SST change applied uniformly.

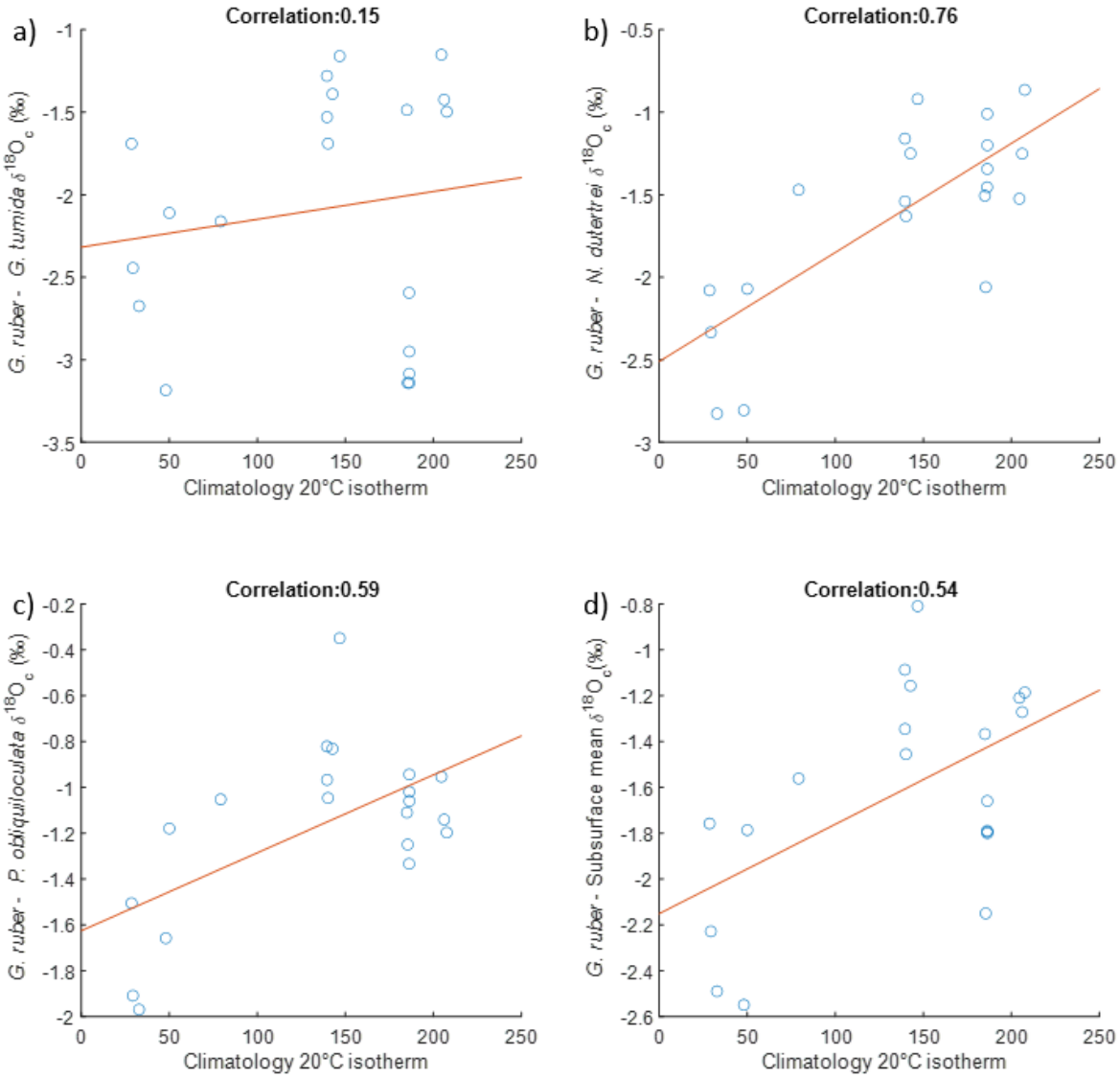

Figure 6: *G. ruber* $\delta^{18}O_c$ compared to subsurface data as a proxy for thermocline depth. a) Climatology 20°C isotherm compared to the difference in $\delta^{18}O_c$ of *G. ruber* and *G. tumida*. b) Same as a) except with *N. dutertrei* in place of *G. tumida*. c) Same as a) except with *P. obliquiloculata* in place of *G. tumida*. d) Same as a) except with the mean of the subsurface species in place of *G. tumida.* Correlation coefficient (R) is indicated on each plot.

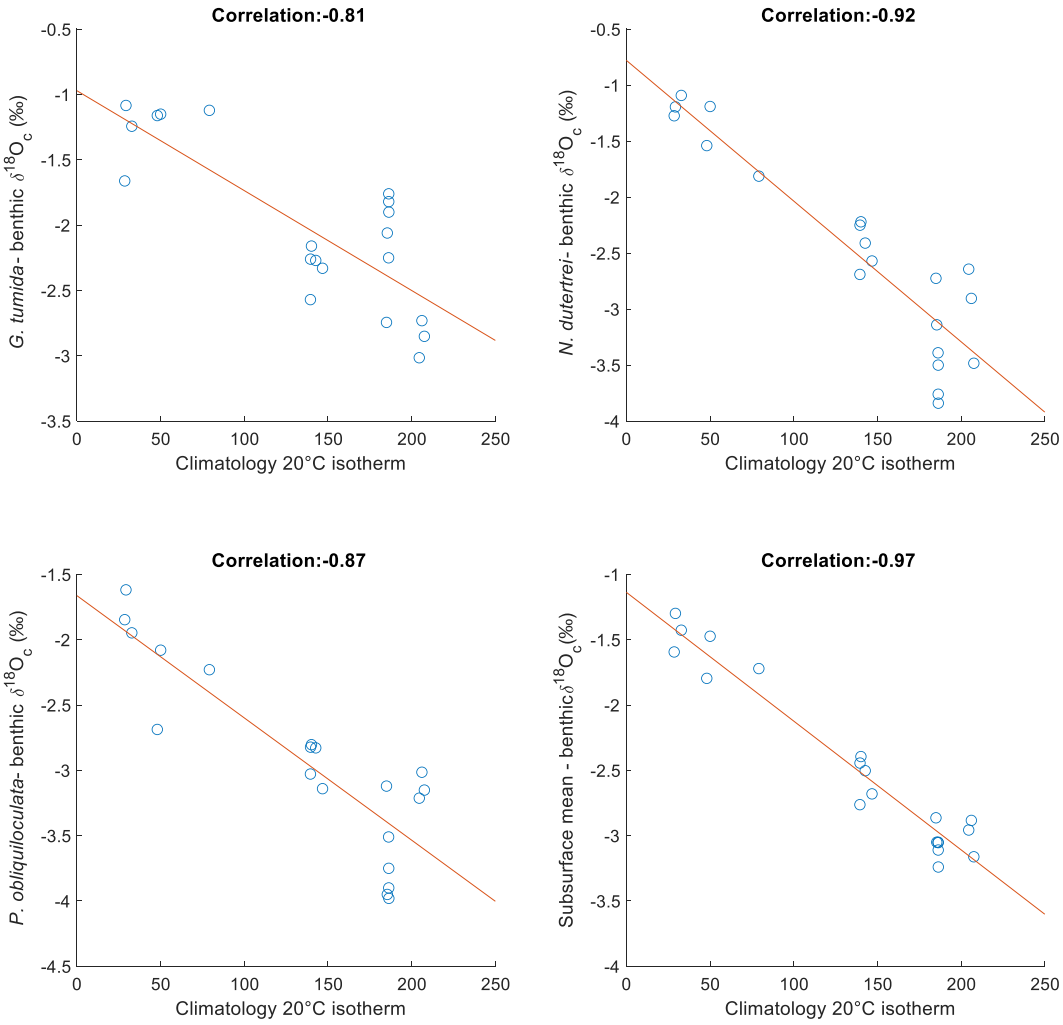

Figure 7: Benthic $\delta^{18}O_c$ compared to subsurface data as a proxy for thermocline depth. Same as Figure 4 except with offset-corrected *U. peregrina* $\delta^{18}O_c$ in place of *G. ruber* $\delta^{18}O_c$.

References

Andreasen, D. J., & Ravelo, A. C. (1997). Tropical Pacific Ocean thermocline depth reconstructions for the Last Glacial Maximum. *Paleoceanography*, *12*(3), 395–413. https://doi.org/10.1029/97PA00822

Bova, S. C., Herbert, T., Rosenthal, Y., Kalansky, J., Altabet, M., Chazen, C., Mojarro, A., & Zech, J. (2015). Links between eastern equatorial Pacific stratification and atmospheric CO2 rise during the last deglaciation. *Paleoceanography*, *30*(11), 1407–1424. https://doi.org/10.1002/2015PA002816

Butzin, M., Köhler, P., & Lohmann, G. (2017). Marine radiocarbon reservoir age simulations for the past 50,000 years. *Geophysical Research Letters*, *44*(16), 8473–8480. https://doi.org/10.1002/2017GL074688

Cannariato, K. G., & Ravelo, A. C. (1997). Pliocene-Pleistocene evolution of eastern tropical surface water circulation and thermocline depth and hemisphere gradient. *Paleoceanography and Paleoclimatology*, *12*(6), 805–820.

Costa, K. M., McManus, J. F., Anderson, R. F., Ren, H., Sigman, D. M., Winckler, G., Fleisher, M. Q., Marcantonio, F., & Ravelo, A. C. (2016). No iron fertilization in the equatorial Pacific Ocean during the last ice age. *Nature*, *529*(7587), 519–522. https://doi.org/10.1038/nature16453

Costa, Kassandra M., Jacobel, A. W., McManus, J. F., Anderson, R. F., Winckler, G., & Thiagarajan, N. (2017). Productivity patterns in the equatorial Pacific over the last 30,000 years. *Global Biogeochemical Cycles*, *31*(5), 850–865. https://doi.org/10.1002/2016GB005579

DiNezio, P. N., Clement, A., Vecchi, G. A., Soden, B., Broccoli, A. J., Otto-Bliesner, B. L., &

509 Braconnot, P. (2011). The response of the Walker circulation to Last Glacial Maximum
510 forcing: Implications for detection in proxies. *Paleoceanography*, *26*(3), 1–21.
511 https://doi.org/10.1029/2010PA002083
512 Fairbanks, R. G. (1989). A 17,000-year glacio-eustatic sea level record: influence of glacial
513 melting rates on the Younger Dryas event and deep-ocean circulation. *Nature*, *342*(6250),
514 637–642. https://doi.org/10.1038/342637a0
515 Fairbanks, R. G., Sverdlove, M., Free, R., Wiebe, P. H., & Bé, A. W. H. (1982). Vertical
516 distribution and isotopic fractionation of living planktonic foraminifera from the Panama
517 Basin. *Nature*, *298*(5877), 841–844. https://doi.org/10.1038/298841a0
518 Fairbanks, R. G., Wiebe, P. H., & Bé, A. W. H. (1980). Vertical distribution and isotopic
519 composition of living planktonic foraminifera in the western north Atlantic. *Science*,
520 *207*(4426), 61–63. https://doi.org/10.1126/science.207.4426.61
521 Ford, H. L., McChesney, C. L., Hertzberg, J. E., & McManus, J. F. (2018). A Deep Eastern
522 Equatorial Pacific Thermocline During the Last Glacial Maximum. *Geophysical Research*
523 *Letters*, *45*(21), 11,806-11,816. https://doi.org/10.1029/2018GL079710
524 Ford, Heather L., Ravelo, A. C., Dekens, P. S., LaRiviere, J. P., & Wara, M. W. (2015). The
525 evolution of the equatorial thermocline and the early Pliocene El Padre mean state.
526 *Geophysical Research Letters*, *42*(12), 4878–4887. https://doi.org/10.1002/2015GL064215
527 Ford, Heather L., Ravelo, A. C., & Hovan, S. (2012). A deep Eastern Equatorial Pacific
528 thermocline during the early Pliocene warm period. *Earth and Planetary Science Letters*,
529 *355–356*, 152–161. https://doi.org/10.1016/j.epsl.2012.08.027
530 Hollstein, M., Mohtadi, M., Kienast, M., Rosenthal, Y., Groeneveld, J., Oppo, D. W., Southon, J.
531 R., & Lückge, A. (2020). The Impact of Astronomical Forcing on Surface and Thermocline

Variability Within the Western Pacific Warm Pool Over the Past 160 kyr. *Paleoceanography and Paleoclimatology*, *35*(6). https://doi.org/10.1029/2019PA003832

Hollstein, Martina, Mohtadi, M., Rosenthal, Y., Moffa Sanchez, P., Oppo, D., Martínez Méndez, G., Steinke, S., & Hebbeln, D. (2017). Stable Oxygen Isotopes and Mg/Ca in Planktic Foraminifera From Modern Surface Sediments of the Western Pacific Warm Pool: Implications for Thermocline Reconstructions. *Paleoceanography*, *32*(11), 1174–1194. https://doi.org/10.1002/2017PA003122

Hollstein, Martina, Mohtadi, M., Rosenthal, Y., Prange, M., Oppo, D. W., Martínez Méndez, G., Tachikawa, K., Moffa Sanchez, P., Steinke, S., & Hebbeln, D. (2018). Variations in Western Pacific Warm Pool surface and thermocline conditions over the past 110,000 years: Forcing mechanisms and implications for the glacial Walker circulation. *Quaternary Science Reviews*, *201*, 429–445. https://doi.org/10.1016/j.quascirev.2018.10.030

Kim, S. T., & O'Neil, J. R. (1997). Equilibrium and nonequilibrium oxygen isotope effects in synthetic carbonates. *Geochimica et Cosmochimica Acta*, *61*(16), 3461–3475. https://doi.org/10.1016/S0016-7037(97)00169-5

Koutavas, A., & Lynch-Stieglitz, J. (2003). Glacial-interglacial dynamics of the eastern equatorial Pacific cold tongue-Intertropical Convergence Zone system reconstructed from oxygen isotope records. *Paleoceanography*, *18*(4). https://doi.org/10.1029/2003PA000894

Lakhani, K. Q., Lynch-Stieglitz, J., & Monteagudo, M. M. (2022). Constraining calcification habitat using oxygen isotope measurements in tropical planktonic foraminiferal tests from surface sediments. *Marine Micropaleontology*, *170*(November 2021), 102074. https://doi.org/10.1016/j.marmicro.2021.102074

Lakhani, K. Q. (2024). lakhani1118/Thermocline_Reconstruction: Thermocline Reconstruction

v1.0 (Version tag1). [Software] Zenodo. https://doi.org/10.5281/zenodo.10806892

Langner, M., & Mulitza, S. (2019). Technical note: PaleoDataView - A software toolbox for the collection, homogenization and visualization of marine proxy data. *Climate of the Past*, *15*(6), 2067–2072. https://doi.org/10.5194/cp-15-2067-2019

Leech, P. J., Lynch-Stieglitz, J., & Zhang, R. (2013). Western Pacific thermocline structure and the Pacific marine Intertropical Convergence Zone during the Last Glacial Maximum. *Earth and Planetary Science Letters*, *363*, 133–143. https://doi.org/10.1016/j.epsl.2012.12.026

LeGrande, A. N., & Schmidt, G. A. (2006). Global gridded data set of the oxygen isotopic composition in seawater. *Geophysical Research Letters*, *33*(12), 1–5. https://doi.org/10.1029/2006GL026011

Liu, S., Jiang, D., & Lang, X. (2020). The Weakening and Eastward Movement of ENSO Impacts during the Last Glacial Maximum. *Journal of Climate*, *33*(13), 5507–5526. https://doi.org/10.1175/jcli-d-19-0728.1

Locarnini, R. A., Mishonov, A. V., Antonov, J. I., Boyer, T. P., Garcia, H. E., Baranova, O. K., Zweng, M. M., Paver, C. R., Reagan, J. R., Johnson, D. R., Hamilton, M., & Seidov, D. (2013). World Ocean Atlas 2013. Vol. 1: Temperature. *NOAA Atlas NESDIS*, *73*(September), 40. http://www.ncbi.nlm.nih.gov/pubmed/22058116%5Cnhttp://www.bloodjournal.org/cgi/doi/10.1182/blood-2011-06-357442

Loubere, P. (2001). Nutrient and oceanographic changes in the Eastern Equatorial Pacific from the last full glacial to the present. *Global and Planetary Change*, *29*(1–2), 77–98. https://doi.org/10.1016/S0921-8181(00)00085-0

Lynch-Stieglitz, J., Curry, W. B., & Slowey, N. (1999). A geostrophic transport estimate for the

578 Florida Current from the oxygen isotope composition of benthic foraminifera.
579 *Paleoceanography*, *14*(3), 360–373.
580 Lynch-Stieglitz, J., Polissar, P. J., Jacobel, A. W., Hovan, S. A., Pockalny, R. A., Lyle, M.,
581 Murray, R. W., Christina Ravelo, A., Bova, S. C., Dunlea, A. G., Ford, H. L., Hertzberg, J.
582 E., Wertman, C. A., Maloney, A. E., Shackford, J. K., Wejnert, K., & Xie, R. C. (2015).
583 Glacial-interglacial changes in central tropical Pacific surface seawater property gradients.
584 *Paleoceanography*, *30*(5), 423–438. https://doi.org/10.1002/2014PA002746
585 Marchitto, T. M., Curry, W. B., Lynch-Stieglitz, J., Bryan, S. P., Cobb, K. M., & Lund, D. C.
586 (2014). Improved oxygen isotope temperature calibrations for cosmopolitan benthic
587 foraminifera. *Geochimica et Cosmochimica Acta*, *130*, 1–11.
588 https://doi.org/10.1016/j.gca.2013.12.034
589 Monteagudo, M. M., Lynch-Stieglitz, J., Marchitto, T. M., & Schmidt, M. W. (2021). Central
590 Equatorial Pacific Cooling During the Last Glacial Maximum. *Geophysical Research*
591 *Letters*, *48*(3), 1–10. https://doi.org/10.1029/2020GL088592
592 Patrick, A., & Thunell, R. C. (1997). *Tropical Pacific sea surface temperature and upper water*
593 *column thermal structure during the last glacial maximum*. *12*(5), 649–657.
594 https://doi.org/https://doi.org/10.1029/97PA01553
595 Ravelo, A. C., & Andreasen, D. H. (1999). Using Planktonic Foraminifera as Monitors of the
596 Tropical Surface Ocean. *Reconstructing Ocean History*, 217–243.
597 https://doi.org/10.1007/978-1-4615-4197-4_14
598 Reimer, P. J., Austin, W. E. N., Bard, E., Bayliss, A., Blackwell, P. G., Bronk Ramsey, C.,
599 Butzin, M., Cheng, H., Edwards, R. L., Friedrich, M., Grootes, P. M., Guilderson, T. P.,
600 Hajdas, I., Heaton, T. J., Hogg, A. G., Hughen, K. A., Kromer, B., Manning, S. W.,

601 Muscheler, R., … Talamo, S. (2020). The IntCal20 Northern Hemisphere Radiocarbon Age
602 Calibration Curve (0-55 cal kBP). *Radiocarbon*, *62*(4), 725–757.
603 https://doi.org/10.1017/RDC.2020.41
604 Rincón-Martínez, D., Steph, S., Lamy, F., Mix, A., & Tiedemann, R. (2011). Tracking the
605 equatorial front in the eastern equatorial Pacific Ocean by the isotopic and faunal
606 composition of planktonic foraminifera. *Marine Micropaleontology*, *79*(1–2), 24–40.
607 https://doi.org/10.1016/j.marmicro.2011.01.001
608 Schrag, D. P., Adkins, J. F., McIntyre, K., Alexander, J. L., Hodell, D. A., Charles, C. D., &
609 McManus, J. F. (2002). The oxygen isotopic composition of seawater during the Last
610 Glacial Maximum. *Quaternary Science Reviews*, *21*(1–3), 331–342.
611 https://doi.org/10.1016/S0277-3791(01)00110-X
612 Spero, H. J., Mielke, K. M., Kalve, E. M., Lea, D. W., & Pak, D. K. (2003). Multispecies
613 approach to reconstructing eastern equatorial Pacific thermocline hydrography during the
614 past 360 kyr. *Paleoceanography*, *18*(1). https://doi.org/10.1029/2002PA000814
615 Tian, Z., & Jiang, D. (2020). Weakening and eastward shift of the tropical Pacific Walker
616 circulation during the Last Glacial Maximum. *Boreas*, *49*(1), 200–210.
617 https://doi.org/10.1111/bor.12417
618 Vecchi, G. A., Soden, B. J., Wittenberg, A. T., Held, I. M., Leetmaa, A., & Harrison, M. J.
619 (2006). Weakening of tropical Pacific atmospheric circulation due to anthropogenic forcing.
620 *Nature*, *441*(1), 73–76. https://doi.org/10.1038/nature04744
621 Wara, M. W., Ravelo, A. C., & Delaney, M. L. (2005). Climate change: Permanent El Niño-like
622 conditions during the Pliocene warm period. *Science*, *309*(5735), 758–761.
623 https://doi.org/10.1126/science.1112596

624

Paleoceanography and Paleoclimatology

Supporting Information for

Reconstructing the Tropical Thermocline from Oxygen-Isotopes in Planktonic and Benthic Foraminifera

K. Q. Lakhani[1], J. Lynch-Stieglitz[1], and B. Findley[1]

[1]Georgia Institute of Technology.

Contents of this file

Figures S1 to S6
Tables S1 to S3

Introduction

This file includes a figure exploring the parameter space of the regression model (Figure S1), figures showing the reconstructed thermocline profiles for all the application of the profile regression method on the other cores from the dataset (Figures S2 – S5), and a figure showing the correlation between the depth of the 20°C isototherm and $\delta^{18}O_c$ = -.66 thermocline metrics (Figure S6). Tables contain the new oxygen isotope data generated from this research (Table S1), the recalibrated radiocarbon dates (Table S2) and the number of analyses contributing to each average value (Table S3).

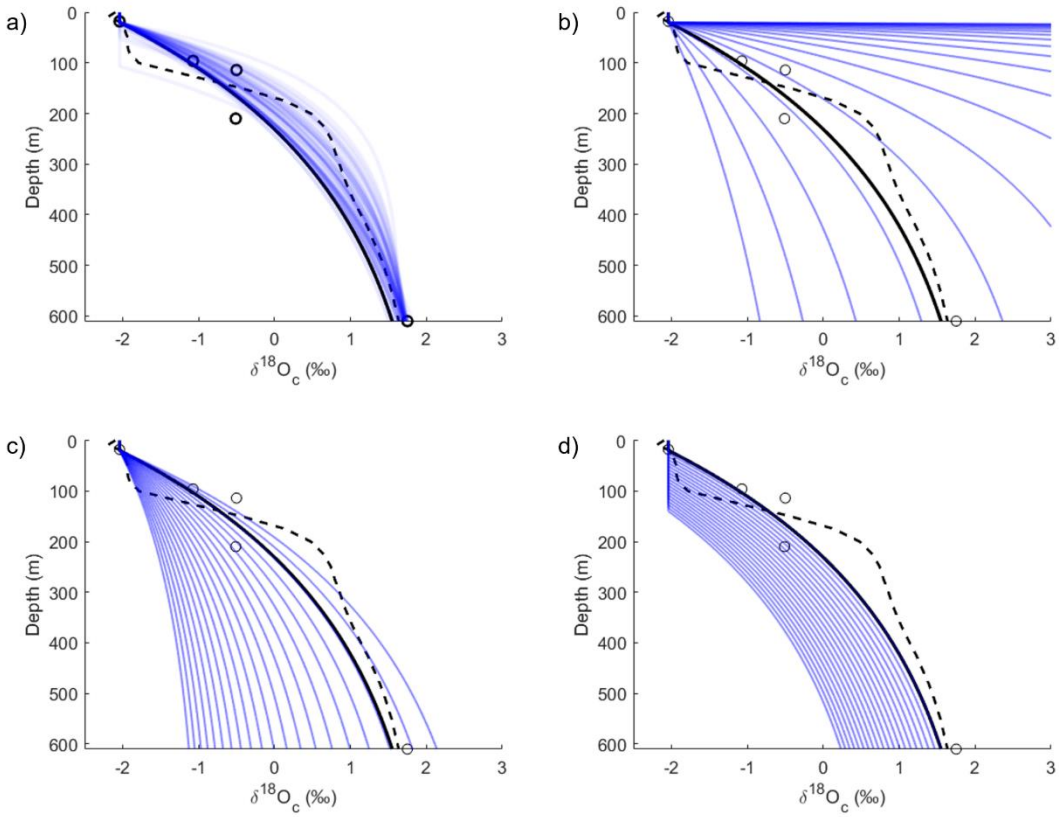

Figure S1. Range of model parameters for this regression model. a) Thermocline model result for ML1208-19GC. Black is the mean regression profile, the dashed line is the climatology profile, and the blue lines indicate MC error due to variability in ACD. b) Average profile with different values for β_1, indicating how β_1 affects profile. Black is average profile, and blue is with a different value of β_1. c) same as b) but for β_2. d) same as b) but for MLD.

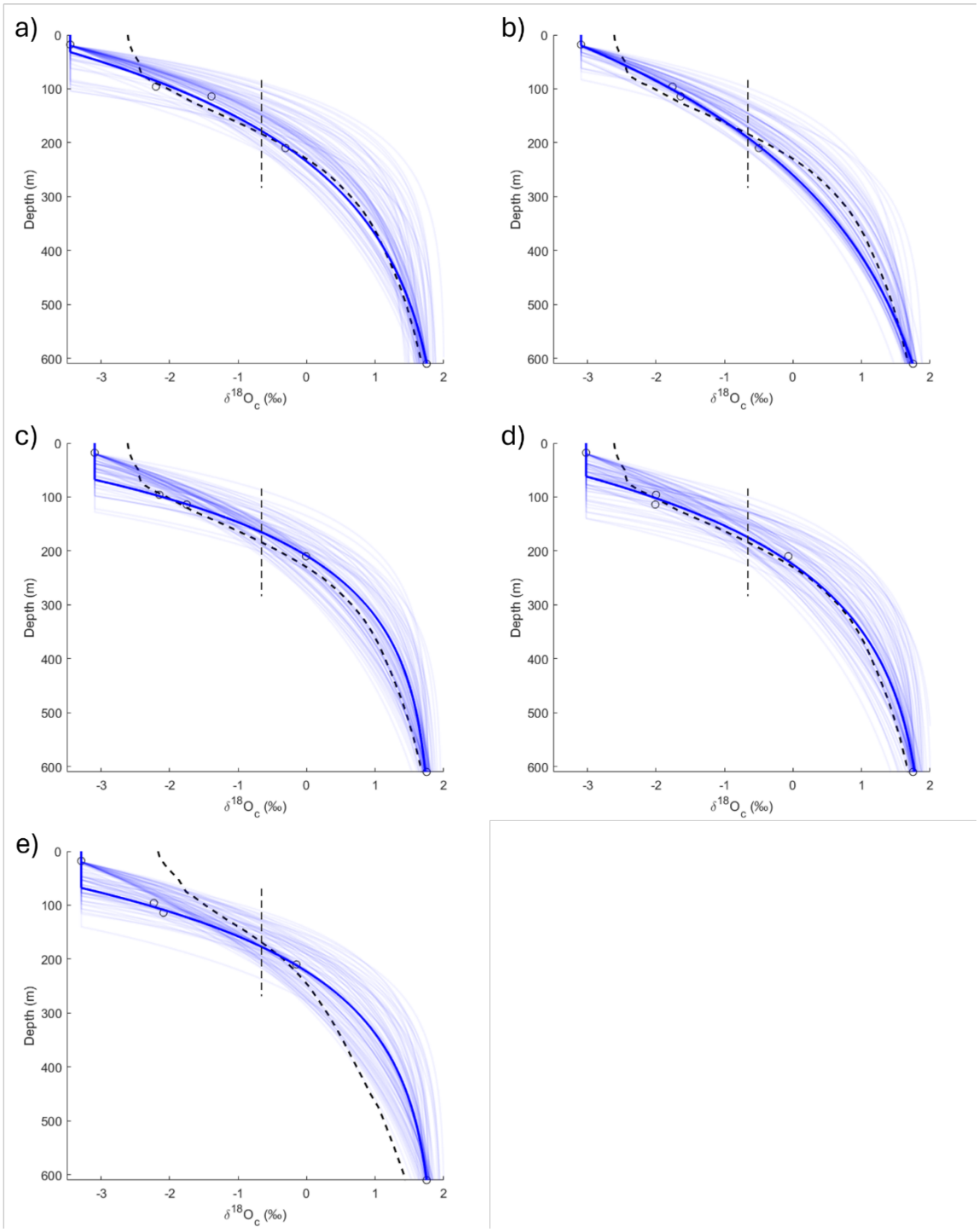

Figure S2. Regression model results from Western Pacific cores off Papua New Guinea. a) Data for core GeoB17421-2 plotted in circles, solid line is profile generated using mean calcification depths, and individual light lines are generated from choosing calcification depth from species-specific depth distributions. Nearest climatology profile is plotted as the dashed line. b) same as a) for GeoB17419-2. c) same as a) for GeoB17430-2. d) same as a) for GeoB17429-1. e) same as a) for GeoB17435-2

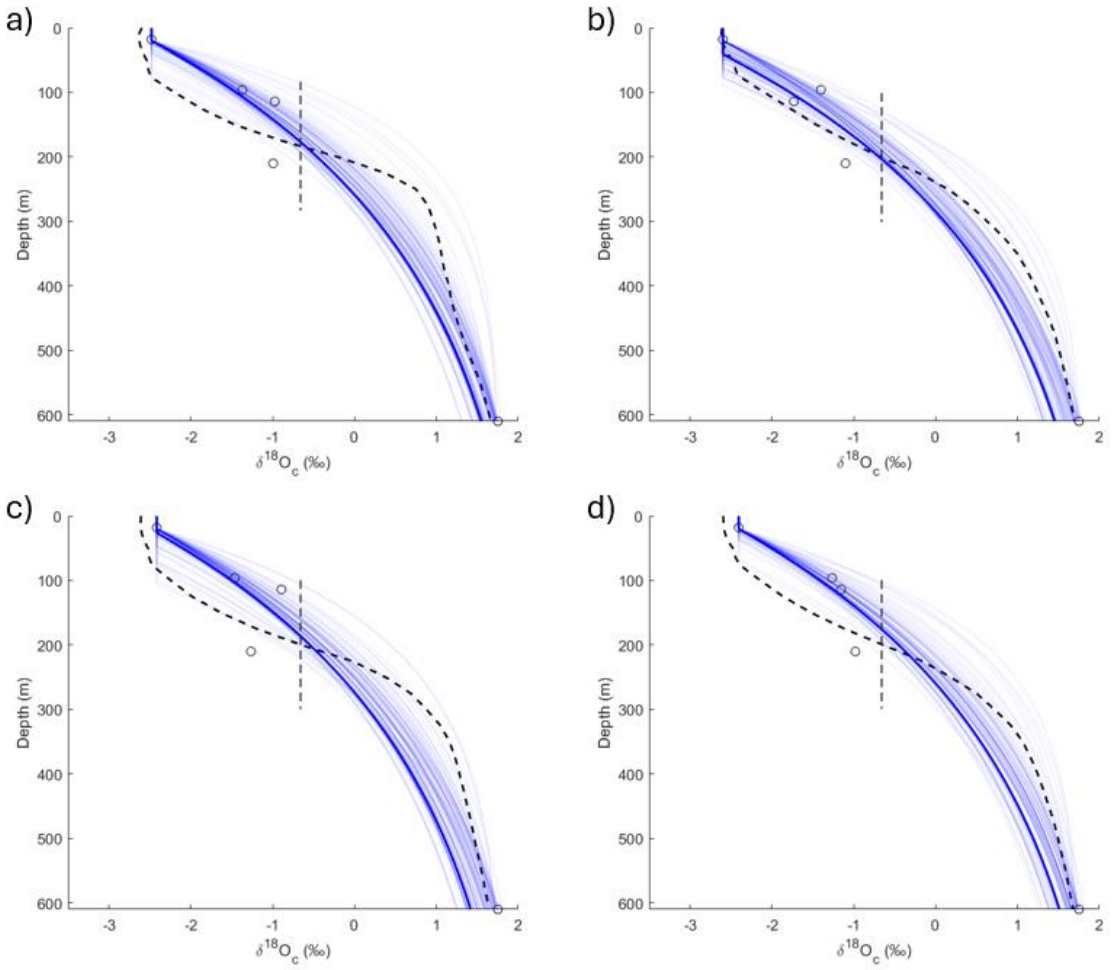

Figure S3. Regression model results from open ocean Western Pacific cores. a) Data for core VM24-150 plotted in circles, solid line is profile generated using mean calcification depths, and individual light lines are generated from choosing calcification depth from species-specific depth distributions. Nearest climatology profile is plotted as the dashed line. b) same as a) for VM28-234. c) same as a) for VM28-235. d) same as a) for VM28-233

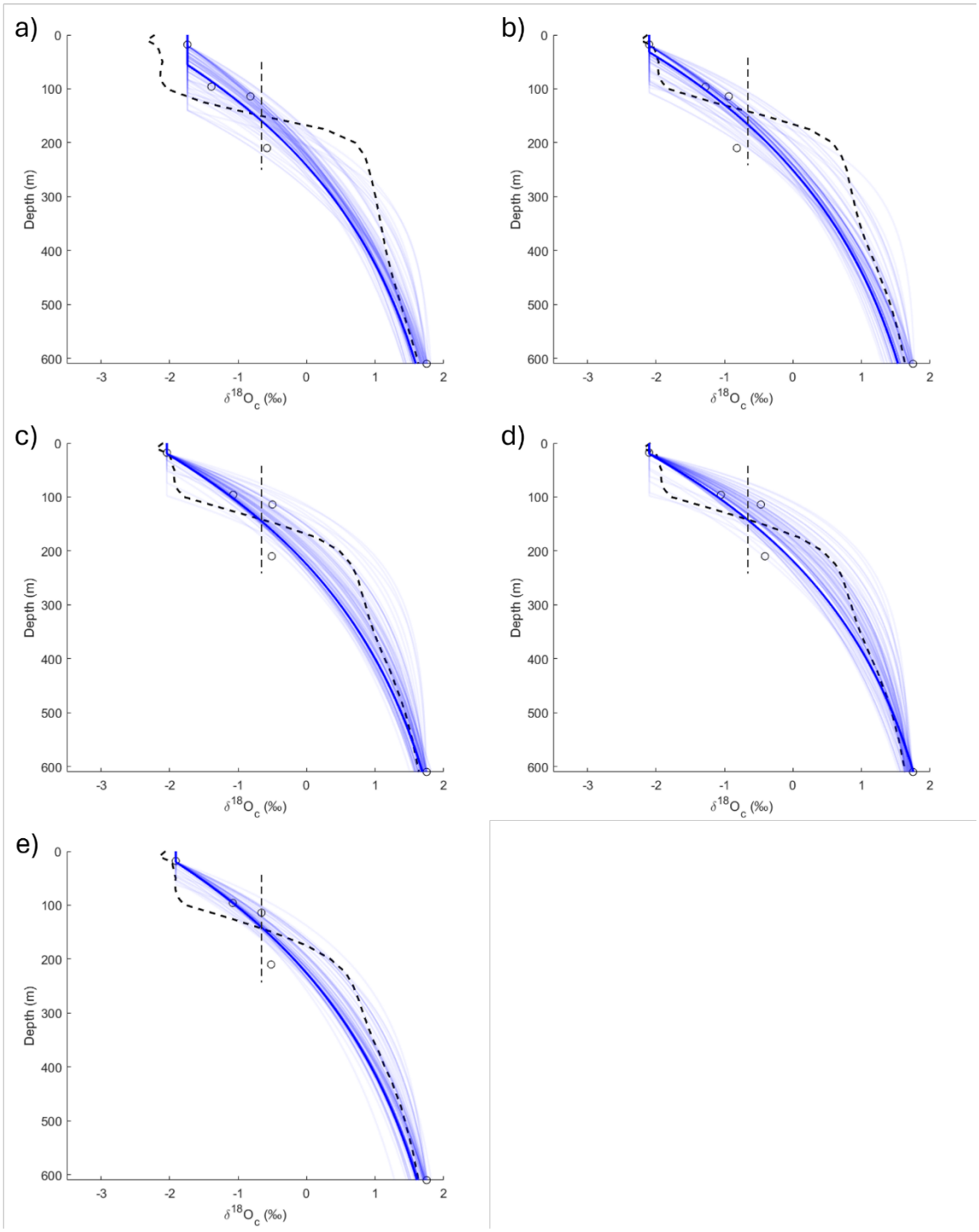

Figure S4. Regression model results from Central Pacific cores. a) Data for core ML1208-28BB plotted in circles, solid line is profile generated using mean calcification depths, and individual light lines are generated from choosing calcification depth from species-specific depth distributions. Nearest climatology profile is plotted as the dashed line. b) same as a) for ML1208-20BB. c) same as a) for ML1208-19GC. d) same as a) for ML1208-18GC. e) same as a) for ML1208-13BB.

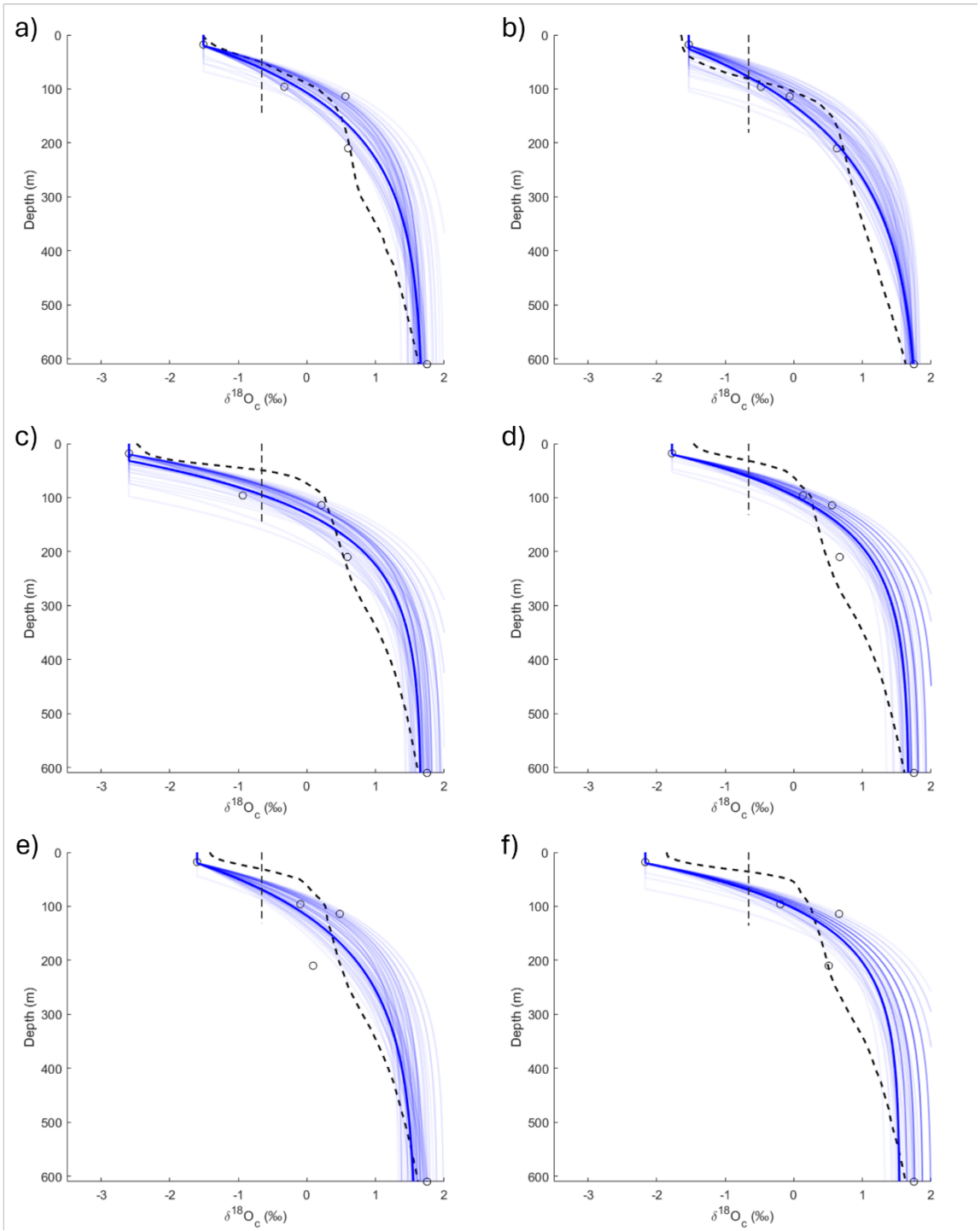

Figure S5. Regression model results from Eastern Pacific cores. a) Data for core ODP 849 plotted in circles, solid line is profile generated using mean calcification depths, and individual light lines are generated from choosing calcification depth from species-specific depth distributions. Nearest climatology profile is plotted as the dashed line. b) same as a) for V21-40. c) same as a) for RC13-140. d) same as a) for RC8-102. e) same as a) for RC11-238. f) same as a) for V19-27.

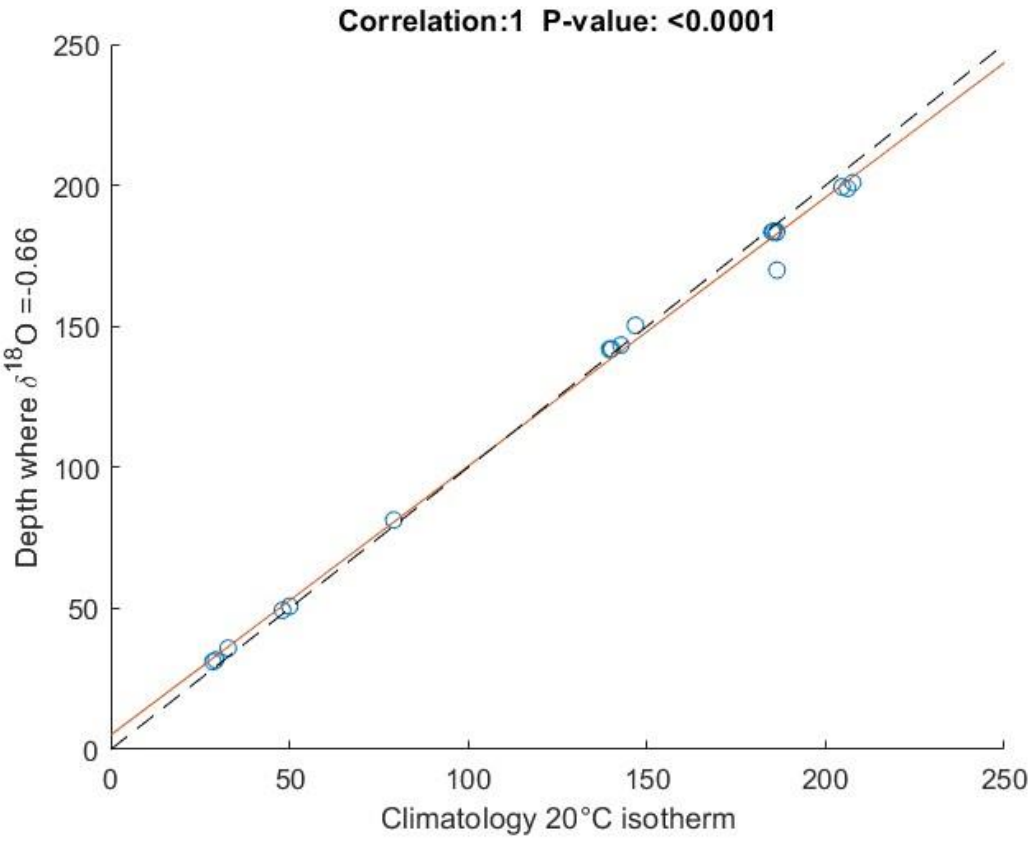

Figure S6. Correlation between Z20 derived from WOA temperature climatology and the depth where climatology-derived $\delta^{18}O$ = -0.66‰. The slope of the line of best fit is 0.95, and the intercept is 5.11 m.

Table S1. Radiocarbon dates with updated calendar age

Core	Core depth (cm)	14C age	Error	Updated Calendar Age (yr BP)	Species	Source
V24-150	4	2520	35	2117	*G. tumida*	Leech et al. 2013
	32	16150	100	19088	*G. tumida*	Leech et al. 2013
	44	19750	85	23365	*G. tumida*	Leech et al. 2013
VM28-234	0	1840	30	1344	*G. tumida*	Leech et al. 2013
	86	13150	55	15134	*T. sacculifer*	Leech et al. 2013
	106	15350	85	18287	*G. tumida*	Leech et al. 2013
	110	14900	75	17709	*T. sacculifer/G. ruber*	Leech et al. 2013
	118	16400	95	1932	*G. tumida*	Leech et al. 2013
	180	20800	210	24549	*G. tumida*	Leech et al. 2013
VM28-235 TW	2	3660	35	3494	*G. tumida*	Leech et al. 2013
VM28-235	28	17300	70	20419	*G. tumida*	Leech et al. 2013
	40	23300	100	27202	*G. tumida*	Leech et al. 2013
VM28-233	1	2270	35	1813	*G. tumida*	Leech et al. 2013
	28	15800	85	18651	*G. tumida*	Leech et al. 2013
	48	22600	150	26508	*G. tumida*	Leech et al. 2013
ML1208-28BB	0	4420	20	4492	*T. sacculifer*	Monteagudo 2022
	8	5950	25	6345	*G. ruber*	Costa et al. 2017
	24	8460	25	8967	*G. ruber*	Costa et al. 2017
	34	10550	30	11834	*G. ruber*	Costa et al. 2017
	46	13550	40	15782	*G. ruber*	Costa et al. 2017
	54	16600	60	19564	*G. ruber*	Costa et al. 2016
	76	25400	160	29323	*G. ruber*	Costa et al. 2016
ML1208-20BB	0	3860	30	3759	*G. ruber*	Lynch-Stieglitz et al. 2015
	7	5380	20	5742	*G. ruber*	Costa et al. 2017
	27	11400	30	12950	*G. ruber*	Costa et al. 2017
	34	13050	30	14938	*G. ruber*	Costa et al. 2017
	40	14685	40	17450	*G. ruber*	Costa et al. 2016
	55	19100	70	22651	*G. ruber*	Costa et al. 2016
ML1208-19GC	0	3120	35	2844	*G. ruber*	Lynch-Stieglitz et al. 2015
	28.5	8510	35	9022	*T. sacculifer*	Monteagudo 2022
	48.5	14550	70	17235	*G. ruber*	Monteagudo 2022
	60.5	20400	150	24087	*T. sacculifer*	Monteagudo 2022

ML1208-18GC	0	3320	45	3092	*T. sacculifer*	Lynch-Stieglitz et al. 2015
	16	5530	60	5901	*G. ruber*	Lynch-Stieglitz et al. 2015
	32	8900	55	9519	*G. ruber*	Lynch-Stieglitz et al. 2015
	48	9800	40	10697	*G. ruber*	Lynch-Stieglitz et al. 2015
	60	13750	90	16077	*G. ruber*	Lynch-Stieglitz et al. 2015
	68	15250	60	18130	*G. ruber*	Lynch-Stieglitz et al. 2015
	92	22500	130	26393	*T. sacculifer*	Monteagudo 2022
	112	28500	130	32226	*G. ruber*	Lynch-Stieglitz et al. 2015
	140	33200	250	37294	*G. ruber*	Lynch-Stieglitz et al. 2015
ML1208-13BB	0	4780	45	5007	*G. ruber*	Lynch-Stieglitz et al. 2015
	11	5960	20	6356	*G. ruber*	Costa et al. 2017
	20	9640	30	10484	*G. ruber*	Costa et al. 2017
	28	11650	30	13140	*G. ruber*	Costa et al. 2017
	34	14580	40	17281	*G. ruber*	Costa et al. 2016
	53	20760	70	24497	*G. ruber*	Costa et al. 2016
V21-40	0	2700	30	2154	*N. dutertrei*	Koutavas and Lynch-Stieglitz 2003
	50	10000	45	10719	*N. dutertrei*	Koutavas and Lynch-Stieglitz 2003
	78	16250	60	18489	*N. dutertrei*	Koutavas and Lynch-Stieglitz 2003
	120	25700	110	28915	*N. dutertrei*	Koutavas and Lynch-Stieglitz 2003
RC13-140	0	1750	25	1018	*N. dutertrei*	Koutavas and Lynch-Stieglitz 2003
	50	10450	45	11356	*N. dutertrei*	Koutavas and Lynch-Stieglitz 2003
	100	16850	55	19278	*N. dutertrei*	Koutavas and Lynch-Stieglitz 2003
	151	24300	85	27500	*N. dutertrei*	Koutavas and Lynch-Stieglitz 2003
RC8-102	0	5150	30	5140	*N. dutertrei*	Koutavas and Lynch-Stieglitz 2003
	49	14000	55	15869	*N. dutertrei*	Koutavas and Lynch-Stieglitz 2003
	101	20100	65	23026	*N. dutertrei*	Koutavas and Lynch-Stieglitz 2003
RC11-238	0	3570	60	3075	*N. dutertrei*	Koutavas and Lynch-Stieglitz 2003
	40	8210	50	8303	*N. dutertrei*	Koutavas and Lynch-Stieglitz 2003
	80	14180	70	16048	*N. dutertrei*	Koutavas and Lynch-Stieglitz 2003
	100	17100	60	19446	*N. dutertrei*	Koutavas and Lynch-Stieglitz 2003

V19-27	0	1340	25	566	*N. dutertrei*	Koutavas and Lynch-Stieglitz 2003
	49	5710	30	5701	*N. dutertrei*	Koutavas and Lynch-Stieglitz 2003
	90	14200	65	16047	*N. dutertrei*	Koutavas and Lynch-Stieglitz 2003
	150	26300	140	29535	*N. dutertrei*	Koutavas and Lynch-Stieglitz 2003

Table S2. New data generated for this study

Core name	Latitude (°N)	Longitude (°W)	Elevation (m)	Depth (cm)	Date	Species	$\delta^{18}O_c$ (‰)	Number of shells	Mass (µg)
ML1208-14MC6	-0.22	-155.96	3049	0	10/25/2021	*P. obliquiloculata*	-0.926	4	159
ML1208-14MC6	-0.22	-155.96	3049	0	10/25/2021	*P. obliquiloculata*	-1.312	4	136
ML1208-14MC6	-0.22	-155.96	3049	0	10/25/2021	*P. obliquiloculata*	-1.080	4	131
ML1208-21MC6	1.27	-157.26	2850	0	10/25/2021	*P. obliquiloculata*	-1.222	4	135
ML1208-21MC6	1.27	-157.26	2850	0	10/25/2021	*P. obliquiloculata*	-1.242	4	168
ML1208-21MC6	1.27	-157.26	2850	0	10/25/2021	*P. obliquiloculata*	-1.371	4	141
ML1208-26MC6	2.46	-159.39	3545	0	10/25/2021	*P. obliquiloculata*	-1.223	5	144
ML1208-26MC6	2.46	-159.39	3545	0	10/25/2021	*P. obliquiloculata*	-1.313	5	140
ML1208-26MC6	2.46	-159.39	3545	0	10/25/2021	*P. obliquiloculata*	-1.034	5	181
ML1208-29MC3	2.97	-159.20	3152	0	10/25/2021	*P. obliquiloculata*	-1.570	4	145
ML1208-29MC3	2.97	-159.20	3152	0	10/25/2021	*P. obliquiloculata*	-1.366	4	150
ML1208-29MC3	2.97	-159.20	3152	0	10/25/2021	*P. obliquiloculata*	-1.235	4	144
ML1208-33MC7	5.20	-160.43	2933	0	10/25/2021	*P. obliquiloculata*	-1.927	4	121
ML1208-33MC7	5.20	-160.43	2933	0	10/25/2021	*P. obliquiloculata*	-1.295	4	160
ML1208-33MC7	5.20	-160.43	2933	0	10/25/2021	*P. obliquiloculata*	-1.652	4	159
V19-27	-0.47	-82.07	1373	55	7/5/2022	*N. dutertrei*	0.582	4	140
V19-27	-0.47	-82.07	1373	55	7/5/2022	*N. dutertrei*	0.744	4	150
V19-27	-0.47	-82.07	1373	55	7/5/2022	*N. dutertrei*	0.719	4	148
V19-27	-0.47	-82.07	1373	55	7/5/2022	*N. dutertrei*	0.829	4	151
V19-27	-0.47	-82.07	1373	46	7/5/2022	*N. dutertrei*	0.728	3	121
V19-27	-0.47	-82.07	1373	46	7/5/2022	*N. dutertrei*	0.376	3	116
V19-27	-0.47	-82.07	1373	46	7/5/2022	*N. dutertrei*	0.710	4	170
V19-27	-0.47	-82.07	1373	46	7/5/2022	*N. dutertrei*	0.361	3	121
V19-27	-0.47	-82.07	1373	14	7/5/2022	*N. dutertrei*	0.478	5	181
V19-27	-0.47	-82.07	1373	14	7/5/2022	*N. dutertrei*	0.767	4	140

V19-27	-0.47	-82.07	1373	12	7/5/2022	*N. dutertrei*	0.855	3	126
V19-27	-0.47	-82.07	1373	12	7/5/2022	*N. dutertrei*	0.761	4	141
V19-27	-0.47	-82.07	1373	14	7/5/2022	*P. obliquiloculata*	-0.197	5	114
RC8-102	-1.42	-86.85	2180	4	7/5/2022	*N. dutertrei*	0.588	2	126
RC8-102	-1.42	-86.85	2180	4	7/5/2022	*N. dutertrei*	0.568	3	162
RC8-102	-1.42	-86.85	2180	4	7/5/2022	*N. dutertrei*	0.509	4	200
RC8-102	-1.42	-86.85	2180	4	7/5/2022	*N. dutertrei*	0.435	5	201
RC8-102	-1.42	-86.85	2180	8	7/5/2022	*N. dutertrei*	0.699	3	104
RC8-102	-1.42	-86.85	2180	8	7/5/2022	*N. dutertrei*	0.568	4	161
RC8-102	-1.42	-86.85	2180	8	7/5/2022	*N. dutertrei*	0.641	5	157
RC8-102	-1.42	-86.85	2180	8	7/5/2022	*N. dutertrei*	0.505	4	169
RC8-102	-1.42	-86.85	2180	1	7/5/2022	*N. dutertrei*	0.588	4	152
RC8-102	-1.42	-86.85	2180	1	7/5/2022	*N. dutertrei*	0.654	4	160
RC8-102	-1.42	-86.85	2180	1	7/5/2022	*N. dutertrei*	0.559	4	165
RC8-102	-1.42	-86.85	2180	1	7/5/2022	*N. dutertrei*	0.462	4	168
RC8-102	-1.42	-86.85	2180	1	7/5/2022	*N. dutertrei*	0.463	4	180
RC8-102	-1.42	-86.85	2180	1	7/17/2022	*P. obliquiloculata*	-0.351	3	164
RC8-102	-1.42	-86.85	2180	4	7/17/2022	*P. obliquiloculata*	1.216	3	101
RC8-102	-1.42	-86.85	2180	8	7/17/2022	*P. obliquiloculata*	-0.506	4	114
RC8-102	-1.42	-86.85	2180	8	7/17/2022	*P. obliquiloculata*	0.637	4	127
RC8-102	-1.42	-86.85	2180	8	7/17/2022	*P. obliquiloculata*	-0.339	5	117
RC8-102	-1.42	-86.85	2180	8	7/17/2022	*G. tumida*	0.658	2	203
V19-27	-0.47	-82.07	1373	14	8/15/2022	*G. tumida*	0.508	1	112
RC8-102	-1.42	-86.85	2180	4	8/15/2022	*G. tumida*	0.401	1	82
RC8-102	-1.42	-86.85	2180	1	8/15/2022	*G. tumida*	0.941	1	88
V19-28	-2.37	-84.65	2720	16	8/15/2022	*G. tumida*	0.636	1	80
V19-28	-2.37	-84.65	2720	16	8/15/2022	*G. tumida*	-0.250	1	114
V19-28	-2.37	-84.65	2720	16	8/15/2022	*G. tumida*	0.790	1	116
V19-28	-2.37	-84.65	2720	29	8/15/2022	*G. tumida*	0.472	1	77
V19-28	-2.37	-84.65	2720	29	8/15/2022	*G. tumida*	-0.392	1	87
V19-28	-2.37	-84.65	2720	29	8/15/2022	*P. obliquiloculata*	1.631	3	83
V19-28	-2.37	-84.65	2720	25	8/15/2022	*P. obliquiloculata*	1.218	3	86
V19-28	-2.37	-84.65	2720	16	8/15/2022	*P. obliquiloculata*	1.291	6	205
V19-28	-2.37	-84.65	2720	12	8/15/2022	*P. obliquiloculata*	-0.487	3	80
RC11-238	-1.52	-85.82	2573	14	8/15/2022	*P. obliquiloculata*	1.263	6	160
RC11-238	-1.52	-85.82	2573	14	8/15/2022	*G. tumida*	-0.063	1	96
RC11-238	-1.52	-85.82	2573	14	8/15/2022	*N. dutertrei*	0.387	4	186
RC11-238	-1.52	-85.82	2573	14	8/15/2022	*P. obliquiloculata*	-0.392	7	175
RC13-140	2.87	-87.75	2246	7	1/21/2023	*P. obliquiloculata*	-1.293	3	78
RC13-140	2.87	-87.75	2246	7	1/21/2023	*P. obliquiloculata*	-1.153	4	82
RC13-140	2.87	-87.75	2246	7	1/21/2023	*P. obliquiloculata*	-0.835	4	83

RC13-140	2.87	-87.75	2246	7	1/21/2023	*N. dutertrei*	0.052	5	179
RC13-140	2.87	-87.75	2246	7	1/21/2023	*N. dutertrei*	0.124	4	136
RC13-140	2.87	-87.75	2246	7	1/21/2023	*N. dutertrei*	-0.008	5	184
RC13-140	2.87	-87.75	2246	3	1/21/2023	*N. dutertrei*	0.417	5	194
RC13-140	2.87	-87.75	2246	3	1/21/2023	*N. dutertrei*	0.398	5	180
RC13-140	2.87	-87.75	2246	3	1/21/2023	*N. dutertrei*	0.081	4	149
RC13-140	2.87	-87.75	2246	3	1/21/2023	*P. obliquiloculata*	-0.840	4	85
RC13-140	2.87	-87.75	2246	3	1/21/2023	*G. tumida*	-0.087	1	94
RC13-140	2.87	-87.75	2246	3	1/21/2023	*G. tumida*	0.631	1	130
RC13-140	2.87	-87.75	2246	7	1/25/2023	*G. tumida*	0.420	1	118
RC13-140	2.87	-87.75	2246	7	1/25/2023	*G. tumida*	0.318	1	138
RC11-238	-1.52	-85.82	2573	19	1/25/2023	*N. dutertrei*	0.521	4	160
RC11-238	-1.52	-85.82	2573	19	1/25/2023	*N. dutertrei*	0.552	4	150
RC11-238	-1.52	-85.82	2573	19	1/25/2023	*N. dutertrei*	0.591	4	146
RC11-238	-1.52	-85.82	2573	19	1/25/2023	*N. dutertrei*	0.336	4	171
RC11-238	-1.52	-85.82	2573	19	1/25/2023	*P. obliquiloculata*	-0.774	2	62
RC11-238	-1.52	-85.82	2573	19	1/25/2023	*P. obliquiloculata*	-0.481	3	74
RC11-238	-1.52	-85.82	2573	19	1/25/2023	*G. tumida*	0.356	1	127
RC11-238	-1.52	-85.82	2573	19	1/25/2023	*G. tumida*	-0.026	1	115
V21-40	-5.52	-106.77	3182	21	2/3/2023	*G. tumida*	0.600	1	112
V21-40	-5.52	-106.77	3182	21	2/3/2023	*N. dutertrei*	-0.089	4	129
V21-40	-5.52	-106.77	3182	21	2/3/2023	*N. dutertrei*	-0.002	5	186
V21-40	-5.52	-106.77	3182	21	2/3/2023	*N. dutertrei*	-0.109	4	145
V21-40	-5.52	-106.77	3182	21	2/3/2023	*P. obliquiloculata*	-0.462	4	75
V21-40	-5.52	-106.77	3182	21	2/3/2023	*P. obliquiloculata*	-0.253	5	127
V21-40	-5.52	-106.77	3182	21	2/3/2023	*P. obliquiloculata*	-0.801	4	115
V21-40	-5.52	-106.77	3182	21	2/6/2023	*G. tumida*	0.935	1	105
V21-40	-5.52	-106.77	3182	21	2/6/2023	*G. tumida*	1.033	1	137
V21-40	-5.52	-106.77	3182	21	2/6/2023	*G. tumida*	-0.115	1	113
V21-40	-5.52	-106.77	3182	21	2/6/2023	*G. tumida*	0.600	1	116
V21-40	-5.52	-106.77	3182	21	2/6/2023	*G. tumida*	0.963	1	111
V21-40	-5.52	-106.77	3182	21	2/6/2023	*G. tumida*	0.477	1	93
RC13-140	2.87	-87.75	2246	24	2/15/2023	*G. tumida*	0.960	1	116
RC13-140	2.87	-87.75	2246	24	2/15/2023	*G. tumida*	1.265	1	95
V21-40	-5.52	-106.77	3182	25	2/16/2023	*N. dutertrei*	0.041	4	135
V21-40	-5.52	-106.77	3182	25	2/16/2023	*N. dutertrei*	0.088	4	173

V21-40	-5.52	-106.77	3182	25	2/16/2023	*P. obliquiloculata*	-0.403	6	155
V21-40	-5.52	-106.77	3182	25	2/16/2023	*G. tumida*	0.537	1	113
V21-40	-5.52	-106.77	3182	25	2/16/2023	*G. tumida*	0.477	1	135
V21-40	-5.52	-106.77	3182	25	2/16/2023	*G. tumida*	0.750	1	99
V21-40	-5.52	-106.77	3182	25	2/16/2023	*G. tumida*	0.861	1	79
V21-40	-5.52	-106.77	3182	25	2/16/2023	*G. tumida*	0.432	1	125
RC13-140	2.87	-87.75	2246	28	2/16/2023	*G. tumida*	0.747	1	117
RC13-140	2.87	-87.75	2246	28	2/16/2023	*G. tumida*	0.234	1	108
RC13-140	2.87	-87.75	2246	28	2/16/2023	*G. tumida*	0.514	1	132
RC13-140	2.87	-87.75	2246	28	2/16/2023	*G. tumida*	0.891	1	98
RC13-140	2.87	-87.75	2246	28	2/16/2023	*P. obliquiloculata*	-0.931	6	161
RC13-140	2.87	-87.75	2246	28	2/16/2023	*P. obliquiloculata*	-0.840	5	97
RC13-140	2.87	-87.75	2246	28	2/16/2023	*N. dutertrei*	0.486	4	173
RC13-140	2.87	-87.75	2246	28	2/16/2023	*N. dutertrei*	0.052	4	162
RC13-140	2.87	-87.75	2246	24	2/16/2023	*N. dutertrei*	0.287	4	161
RC13-140	2.87	-87.75	2246	24	2/16/2023	*N. dutertrei*	0.333	4	142
RC13-140	2.87	-87.75	2246	24	2/16/2023	*N. dutertrei*	0.098	4	167
RC13-140	2.87	-87.75	2246	24	2/16/2023	*P. obliquiloculata*	-0.665	5	129
VM28-235	-5.45	160.48	1746	2	2/25/2023	*P. obliquiloculata*	-1.514	4	192
VM28-235	-5.45	160.48	1746	2	2/25/2023	*P. obliquiloculata*	-1.234	4	156
VM28-235	-5.45	160.48	1746	2	2/25/2023	*N. dutertrei*	-0.703	4	146
VM28-235	-5.45	160.48	1746	2	2/25/2023	*N. dutertrei*	-0.863	4	167
VM28-235	-5.45	160.48	1746	2	2/25/2023	*N. dutertrei*	-1.113	4	140
VM28-234	-7.13	158.97	2719	0	2/25/2023	*N. dutertrei*	-1.612	4	117
VM28-234	-7.13	158.97	2719	0	2/25/2023	*N. dutertrei*	-1.855	4	107
VM28-233	-6.32	161.38	2334	4	2/25/2023	*N. dutertrei*	-1.616	4	133
VM28-233	-6.32	161.38	2334	4	2/25/2023	*N. dutertrei*	-0.877	4	160
VM28-233	-6.32	161.38	2334	4	2/25/2023	*N. dutertrei*	-0.970	4	116
V24-150	-2.20	155.70	1849	0	2/25/2023	*N. dutertrei*	-0.827	4	136
V24-150	-2.20	155.70	1849	0	2/25/2023	*N. dutertrei*	-0.999	4	170
V24-150	-2.20	155.70	1849	0	2/25/2023	*N. dutertrei*	-1.333	4	162
ML1208-19GC	0.83	-156.87	2956	0	2/26/2023	*P. obliquiloculata*	-0.996	4	141
ML1208-18GC	0.59	-156.66	3362	0	2/26/2023	*P. obliquiloculata*	-0.979	4	126
ML1208-18GC	0.59	-156.66	3362	0	2/26/2023	*P. obliquiloculata*	-1.520	4	131

ML1208-18GC	0.59	-156.66	3362	0	2/26/2023	*P. obliquiloculata*	-1.252	4	118
ML1208-18GC	0.59	-156.66	3362	4	2/26/2023	*P. obliquiloculata*	-0.997	5	169
ML1208-18GC	0.59	-156.66	3362	4	2/26/2023	*P. obliquiloculata*	-0.722	5	162
ML1208-18GC	0.59	-156.66	3362	4	2/26/2023	*P. obliquiloculata*	-0.889	4	129
ML1208-13BB	-0.22	-155.96	3050	4	2/26/2023	*P. obliquiloculata*	-1.164	4	157
ML1208-13BB	-0.22	-155.96	3050	4	2/26/2023	*P. obliquiloculata*	-0.980	4	137
ML1208-13BB	-0.22	-155.96	3050	4	2/26/2023	*P. obliquiloculata*	-0.841	4	103
ML1208-13BB	-0.22	-155.96	3050	4	2/26/2023	*P. obliquiloculata*	-1.374	4	123
VM28-235	-5.45	160.48	1746	2	2/26/2023	*P. obliquiloculata*	-1.500	3	133
VM28-235	-5.45	160.48	1746	2	2/26/2023	*P. obliquiloculata*	-1.605	3	137
ML1208-19GC	0.83	-156.87	2956	0	3/17/2023	*P. obliquiloculata*	-1.158	4	149
ML1208-19GC	0.83	-156.87	2956	0	3/17/2023	*P. obliquiloculata*	-1.064	4	168
ML1208-13BB	-0.22	-155.96	3050	0	3/17/2023	*P. obliquiloculata*	-1.085	3	125
ML1208-13BB	-0.22	-155.96	3050	0	3/17/2023	*P. obliquiloculata*	-1.106	4	137
ML1208-13BB	-0.22	-155.96	3050	0	3/17/2023	*P. obliquiloculata*	-1.062	4	141
ML1208-13BB	-0.22	-155.96	3050	0	3/17/2023	*P. obliquiloculata*	-1.125	4	152
VM28-229	-8.40	167.77	3669	0	3/18/2023	*P. obliquiloculata*	-1.358	4	179
V24-150	-2.20	155.70	1849	8	3/18/2023	*N. dutertrei*	-0.381	4	144
V24-150	-2.20	155.70	1849	8	3/18/2023	*N. dutertrei*	-0.949	5	154
V24-150	-2.20	155.70	1849	8	3/18/2023	*N. dutertrei*	-1.115	5	165

Table S3: Number of individuals (n) contributing to the averages in Table 1

Core name	Latitude (°N)	Longitude (°E)	Depth (m)	G. ruber n	G. tumida n	N. dutertrei n	P. obliq n
GeoB17421-2	-3.55	144.20	588	3-10[4]	3-10[4]	3-10[4]	3-10[4]
GeoB17419-2	-2.81	144.50	1887	3-10[4]	3-10[4]	3-10[4]	3-10[4]
GeoB17430-2	-4.22	145.03	1160	3-10[4]	3-10[4]	3-10[4]	3-10[4]
GeoB17429-1	-4.10	145.20	1604	3-10[4]	3-10[4]	3-10[4]	3-10[4]
GeoB17435-2	-7.27	147.34	1001	3-10[4]	3-10[4]	3-10[4]	3-10[4]
VM24-150	-2.20	155.70	1849	40[2]	20[2]	26	9[2]
VM28-234	-7.13	158.97	2719	170[2]	78[2]	8	63[2]
VM28-235	-5.45	160.48	1746	30[2]	22[2]	12	14
VM28-233	-6.32	161.38	2334	20[2]	22[2]	12	9[2]
ML1208-28BB	2.97	-159.20	3153	15[3]	8[3]	8[3]	12
ML1208-20BB	1.27	-157.26	2850	15[3]	8[3]	8[3]	12
ML1208-19GC	0.83	-156.87	2956	15[3]	8[3]	8[3]	12
ML1208-18GC	0.59	-156.66	3362	15[3]	8[3]	8[3]	26
ML1208-13BB	-0.22	-155.96	3050	15[3]	8[3]	8[3]	31
ODP 849	0.18	-110.52	3839	10-60[5]	10-60[5]	10-60[5]	10-60[5]
V21-40	-5.52	-106.77	3182	~60[1]	12	21	19
RC13-140	2.87	-87.75	2246	~45[1]	10	48	31
RC8-102	-1.42	-86.85	2180	~15[1]	4	50	19
RC11-238	-1.52	-85.82	2573	~45[1]	3	33	18
V19-27	-0.47	-82.07	1373	~60[1]	1	45	5

[1]Koutavas et al. 2003
[2]Leech et al. 2013
[3]Lynch-Stieglitz et al. 2015
[4]Hollstein et al. 2017
[5]Ford et al. 2018